Synchronous asymmetric exclusion processes

1998 J. Phys. A: Math. Gen. 31 5033

(http://iopscience.iop.org/0305-4470/31/22/008)

J. Phys. A: Math. Gen. **31** (1998) 5033–5063. Printed in the UK PII: S0305-4470(98)90214-1

Synchronous asymmetric exclusion processes

L G Tilstra† and M H Ernst‡

Institute for Theoretical Physics, University of Utrecht, Princetonplein 5, 3584 CC Utrecht, The Netherlands

Received 22 December 1997, in final form 23 March 1998

Abstract. For a fully synchronous asymmetric exclusion process with open or closed boundaries only partial analytic results are known owing to the appearance of strong-short range correlations, which invalidate simple mean-field approximations. Here we present a new method for calculating basic properties of nonequilibrium steady states, and calculate densities, fluxes, travel times, spatial and temporal correlation functions, phase diagrams, profiles and widths of boundary layers and interfaces between phases in coexistence, as well as their microstructures.

This paper is based on two new elements: (i) a microscopic characterization of order parameters and local configurations in the relevant phases, based on the microdynamics of the model, and (ii) an improved mean-field approximation, which neglects certain four-point—and higher-order correlation functions. It is *conjectured* that the density profiles, obtained here, are exact up to terms that are exponentially small in the system size.

1. Introduction

Nonequilibrium stationary states (NESS) violate detailed balance, they cannot be described as Gibbs states, and their behaviour shows a wealth of interesting phenomena that are absent in thermal equilibrium, such as boundary-induced phase transitions, self-organization, pattern formation, and long-range spatial and temporal correlations. They occur in classical fluids [1], driven diffusive systems [2–4], granular flows [5] and lattice gas cellular automata (LGCA) with collision rules violating detailed balance [6], of which traffic models [7] are simple examples. Unfortunately, a general theory similar to Gibbs statistical mechanics is lacking for NESS, where results seem much less universal, and depend strongly upon boundary conditions, driving forces, and the (sequential or synchronous) order in which the microscopic dynamics is applied [8].

The standard theoretical approaches are based on Langevin equations, fluctuating hydrodynamics, mode coupling theories, and ring kinetic theory, which are phenomenological and/or approximate in nature. A large amount of theoretical understanding has also been obtained from computer simulations.

However, since 1992 new methods for obtaining exact solutions for simple open one-dimensional systems, the so-called asymmetric exclusion processes, have been developed based on transfer matrix methods (Bethe ansatz, matrix product ansatz [9–19]). One can calculate bulk properties, phase diagrams, density profiles of boundary layers and interfaces between coexisting bulk phases, as well as spatial and temporal correlation functions. The

† E-mail address: tilstra@fys.ruu.nl
‡ E-mail address: ernst@fys.ruu.nl

0305-4470/98/225033+31$19.50

number of exact results is rapidly growing. For an up-to-date list of references to analytic results for asymmetric exclusion processes we refer the reader to [8].

Asymmetric exclusion processes describe (open or closed) systems of interacting particles or random walkers on a lattice, in most cases linear chains, with hard core exclusion for double occupancy, and with hopping rates differing for different directions. The bulk dynamics may be deterministic or stochastic. Open systems are coupled to reservoirs at both ends through stochastic boundaries. Closed systems on a ring are coupled to local randomness such as defect sites [15, 21] or defect particles [16–18]. Applications range from shock waves in the Burgers equation, to traffic flow problems, reaction-diffusion systems and growth models.

The problem can be formulated in terms of master equations with discrete or continuous time [9], or in terms of the equivalent transfer matrices for spin chains [20], or as microdynamic equations, as is usually done in LGCA, when used as models for nonequilibrium fluids [23]. LGCA represent perhaps also a more faithful representation of real traffic problems [7, 17]. The LGCA approach will be followed in this paper.

The dynamics of updating sites may be applied in (random) sequential order, typical for the master equation description, or in parallel, i.e. fully synchronous for all sites, typical for LGCA, or in any intermediate version with strictly sequential or with sublattice–parallel updating [11, 13]. The different ways of updating are an essential part of the model. They affect the existence of different phases in the phase diagram, as well as the structure of the spatial and temporal correlations. For instance, the so-called maximum current phase (see [9]) is present in the totally asymmetric exclusion process (TASEP) with open boundaries, when updating is carried out in random sequential order [9, 10], but is absent for other updating schemes [11, 13, 21, 22]. The spatial correlations are weakest for random sequential updating, intermediate for sequential and sublattice–parallel updatings, and strongest for parallel updating.

As far as analytic approaches are concerned many exact results concerning bulk properties, spatial and temporal correlations, and profiles are known for random sequential and sublattice–parallel updatings [7–9, 11]. The fully parallel updating schemes of LGCA offer the largest difficulties, because the dynamics creates strong short-range correlations, which invalidate simple mean-field approaches. Only some bulk properties such as density, flux and the phase diagram have been obtained [8, 21, 22], where 'in the bulk' means 'outside the boundary layers'.

The main aim of this paper is an analytic calculation of the basic average properties of single particles, and their spatial and temporal correlations in the NESS. Moreover, we derive the profiles and widths of boundary layers and of interfaces between phases in coexistence, as conjectured in [22] for an open TASEP with parallel updating, where the particles move forward (which is from *left* to *right* in our frame of reference) fully synchronously at every timestep with probability $p = 1$ (deterministic bulk dynamics) if their right-nearest-neighbour (r.n.n.) site is empty, and where input and removal rates specify the stochastic boundary conditions. In [8] a much richer stochastic version of the same model with $p < 1$ has been considered, and mean-field results, based on a matrix multiplication ansatz, have been obtained. It includes the deterministic TASEP, discussed in this paper, as a special case. However, even with the highly sophisticated matrix multiplication ansatz, the profiles and correlation functions have not yet been calculated as the associated matrix algebra is quite complicated [8]. In the case of sequential or sublattice updating the model of [8] has already been generalized to include backward jumps with probability q, and input and removal rates at both ends of the chain [12].

Our approach starts in section 2 from the *microdynamic equations*, which describe the

time evolution of the set of occupation numbers $\{\tau_i(t)\}$ of the sites $i = 1, 2, \ldots, L$ on the chain at time t, as a discrete continuity equation, in which all variables are Boolean variables, having only values 0 or 1

$$\tau_i(t+1) - \tau_i(t) = \hat{j}_{i-1}(t) - \hat{j}_i(t). \tag{1}$$

Here the instantaneous microscopic flux $\hat{j}_i(t)$ counts the number of particles passing through link $(i, i+1)$ at time $t = 0, 1, 2, \ldots$. The influx $\hat{j}_0(t)$ and outflux $\hat{j}_L(t)$ specify the couplings to the stochastic reservoirs or blockage sites. Further specification of the fluxes depends on the model, and will be given later.

A detailed analysis of the microscopic evolution equation for sets of particle clusters $\tau_i\tau_{i+1}\ldots$, derived in section 3, allows us not only to determine the short-range correlation functions that are built up through the dynamics, but also to identify the different phases, as well as the microscopic structure of boundary layers and the interface between different bulk phases, without performing any averages. Averages such as bulk densities and flux, as well as the phase diagram are calculated in section 4. The phase diagram shows a phase transition from a free-flow regime ($\alpha < \beta$), where all particles are moving at maximum speed, to a congested or jammed regime ($\alpha > \beta$), where the dynamics is controlled by start–stop waves. Here α is the input rate and β the removal rate. When both rates are equal, there are coexisting phases with a sharp interface (shock wave) between them. The interpretation of the interface as a shock wave forms the direct link with Burgers nonlinear diffusion equation [14].

In section 5 an exact hierarchy for particle-cluster correlation functions is derived, to which we apply our improved mean-field approximation (MFA). It assumes for the low density phase, that *inside the interface* between bulk phase and boundary layer, the higher-order correlations between on the one hand a particle–hole pair, and on the other hand the particle cluster on its r.n.n. site, can be neglected. This is equivalent to neglecting certain four-point correlation functions. For the high-density phase, similar results are obtained through particle–hole symmetry. The MFA reduces the hierarchy to a set of recursion relations for the correlation functions and density profiles, which are solved in this section. Knowledge of the density profile also enables us to calculate the average travel time of particles. The results are new, and are in excellent agreement with extensive computer simulations. The present MFA is similar in spirit, but not in specific details, to the improved MFA of [7] that accounts for short-range two-point correlations, but neglects higher order ones, and that leads to the solution of the TASEP on a ring without a blockage.

To test the validity of our MFA we have applied the method in the appendix to the same open TASEP, but now with sublattice–parallel updating, for which the exact correlations functions have been calculated in [11, 13]. It appears that the results agree with the exact results, apart from terms that are exponentially small in the length of the chain. Moreover, it turns out that spatial correlations arising from parallel updating are quite different from those coming from sublattice–parallel updating.

In section 6 we exploit the analogy that a blockage site on a ring has with on the one hand the entrance site and on the other hand with the exit site of the corresponding open system. In this way we recover the results of [21] for the phase diagram, fluxes and the bulk densities for the TASEP with a blockage on a ring with parallel updating. In addition we are able to construct the higher-order correlation functions, density profiles and finite-size corrections (rounding) of the $j(\rho)$-relation ('equation of state') at the high- and low-density regimes of the coexisting phase region. Again, the results are new and in good agreement with computer simulations. We end section 7 with some conclusions and suggestions.

2. TASEP with synchronous dynamics

2.1. Definitions

We consider a totally asymmetric exclusion process with open boundaries as LGCA, with particles living on a one-dimensional lattice with sites labelled $i = \{1, \ldots, L\}$. The configuration of particles at time $t = 0, 1, 2, \ldots$ is described by the set of occupation numbers $\{\tau_i(t)\}$ with $i = 1, 2, \ldots, L$, where $\tau_i(t) \equiv 1 - \sigma_i(t) = 1$ if the site i is occupied by a particle, and $\tau_i(t) = 0$ if the site is empty, i.e. is occupied by a hole ($\sigma_i(t) = 1$). The dynamics is defined such that all particles, with an *empty* r.n.n. site at time t, simultaneously jump to that site at the next timestep $(t + 1)$. If that site is occupied, the particle does not move. So, the dynamics or updating in the bulk of the system is deterministic and fully parallel.

Next, *boundary conditions* are specified. We consider an open system, coupled to two stochastic reservoirs, one that injects particles with a probability α $(0 < \alpha \leqslant 1)$ into site 1, provided it is empty, and one that removes particles from site L with probability β $(0 < \beta \leqslant 1)$ provided site L is occupied.

Throughout this paper the configurations of the system at time t and $t + 1$ will be denoted by $\tau_i = \tau_i(t)$ and $\tau_i' = \tau_i(t + 1)$. Then, according to the dynamic rules described above, the configuration τ_i' is given by the microdynamic equation $\tau_i' = \tau_i + \hat{\jmath}_{i-1} - \hat{\jmath}_i$ with bulk and boundary fluxes given by†

$$\begin{aligned} &\hat{\jmath}_i = \tau_i\sigma_{i+1} \qquad (i = 1, \ldots, L-1) \\ &\hat{\jmath}_0 = \tau_0\sigma_1 = \hat{\alpha}\sigma_1 \\ &\hat{\jmath}_L = \tau_L\sigma_{L+1} = \hat{\beta}\tau_L. \end{aligned} \tag{2}$$

Here $\hat{\alpha} = \tau_0$ and $\hat{\beta} = \sigma_{L+1}$ represent a set of independent random Boolean variables, which take the values $\{0, 1\}$ with expectations $\langle\hat{\alpha}\rangle = \alpha$ and $\langle\hat{\beta}\rangle = \beta$, and which are drawn at every timestep from a uniform distribution. For later analysis it is convenient to transform the microdynamic equation (1), (2) to hole-occupation numbers $\sigma_i = 1 - \tau_i$, yielding

$$\sigma_i' = \tau_i\sigma_{i+1} + \sigma_{i-1}\sigma_i \qquad (i = 1, \ldots, L). \tag{3}$$

The equations for the time evolution of averages $\langle\tau_i(t)\rangle \equiv \langle\tau_i\rangle_t$, correlation functions $\langle\tau_i\tau_k\rangle_t$ etc, can be derived by multiplying the equations in (1) for different sites and subsequently averaging over arbitrary initial configurations $\{\tau_i(0)\}$. In this way one obtains an open hierarchy which couples the time changes of a correlations function to higher-order ones.

For large times ($t \to \infty$) the system will approach a nonequilibrium stationary state, which is the main focus of attention in this paper. Averages over the NESS are denoted by $\langle\ldots\rangle$. This state is expected to be *unique*, i.e. independent of the initial configuration $\{\tau_i(0)\}$. Therefore in analytical considerations the initial state is always taken to be the *empty* state $\{\tau_i(0) = 0\}$ for all i $(i = 1, 2, \ldots, L)$.

2.2. Symmetries

A quantity of paramount interest is the average flux $\langle\hat{\jmath}_i\rangle$ through the link $(i, i + 1)$,

$$\langle\hat{\jmath}_i\rangle = \langle\tau_i\sigma_{i+1}\rangle \tag{4}$$

† In the model of [8] the boundary fluxes are the same, but the bulk flux is generalized to $\hat{\jmath}_i = \hat{p}_i\tau_i\sigma_{i+1}$, where $\hat{p}_i$ with $\langle\hat{p}_i\rangle = p$ represents a set of independent Boolean variables, similar to $\hat{\alpha}$ and $\hat{\beta}$.

and the local flow velocity or average speed $v_i = \langle \hat{j}_i \rangle / \langle \tau_i \rangle$. In the NESS these averages are independent of time, and the average flux can be calculated from the continuity equation (1), combined with (2) using the relation $\langle \tau_i' \rangle = \langle \tau_i \rangle$. This yields a constant site-independent flux j through the system,

$$\begin{aligned} &\langle \hat{j}_{i-1} \rangle = \langle \hat{j}_i \rangle = \langle \tau_i \sigma_{i+1} \rangle = j \\ &\langle \hat{j}_0 \rangle = \alpha(1 - \langle \tau_1 \rangle) = j \\ &\langle \hat{j}_L \rangle = \beta \langle \tau_L \rangle = j \end{aligned} \tag{5}$$

with $i = 0, 1, \ldots, L$. The flux in the NESS is translationally invariant. Once the nearest-neighbour correlations are known, the density profile can be calculated from (4) with $\sigma_{i+1} = 1 - \tau_{i+1}$, yielding

$$\langle \tau_i \rangle = j + \langle \tau_i \tau_{i+1} \rangle. \tag{6}$$

The equations of motion exhibit particle–hole symmetry, and the *duality transformation*,

$$\begin{aligned} &\tau_i \leftrightarrow \sigma_{L-i+1} \qquad (i = 1, \ldots, L) \\ &\tau_0 = \hat{\alpha} \leftrightarrow \sigma_{L+1} = \hat{\beta} \\ &\hat{j}_i \leftrightarrow \hat{j}_{L-i} \end{aligned} \tag{7}$$

maps the microdynamic equation (1), (2) into the equivalent representation (3), i.e. the microdynamic equation is invariant under particle–hole exchange. Consequently, the average occupation numbers satisfy the symmetry relations

$$\begin{aligned} \langle \tau_i \rangle(\alpha, \beta) &= \langle \sigma_{L-i+1} \rangle(\beta, \alpha) \\ &= 1 - \langle \tau_{L-i+1} \rangle(\beta, \alpha) \end{aligned} \tag{8}$$

with $i = 1, 2, \ldots, L$. As the flux maps $\hat{j}_i \leftrightarrow \hat{j}_{L-i}$ under the duality transformation, the average flux satisfies the symmetry relation $j_i(\alpha, \beta) = j_{L-i}(\beta, \alpha)$. However, the average flux in the NESS is constant for all sites, hence

$$j(\alpha, \beta) = j(\beta, \alpha). \tag{9}$$

The particle–hole symmetry is a very powerful tool, as all properties for $\alpha > \beta$ (high density) can be obtained from those for $\alpha < \beta$ (low density).

3. Dynamics and structures

3.1. Build up of dynamic correlations.

In this section we show that a qualitative analysis of the dynamics and instantaneous configurations—without performing any averaging—leads already to the complete phase diagram, to an identification of the relevant order parameters, and to a qualitative characterization of the structure of the high- and low-density phase, as well as to the typical dynamics in the different phases.

In the following we will consider the dynamics of *clusters* of particles and holes described in terms of the Boolean variables,

$$\begin{aligned} T_{kl} &= \tau_k \tau_{k+1} \ldots \tau_l \\ S_{kl} &= \sigma_k \sigma_{k+1} \ldots \sigma_l \end{aligned} \tag{10}$$

with $k < l$, i.e. a cluster has at least two constituents. The time evolution equations for these objects are obtained by multiplying (1) from k to l, using $\sigma_j \tau_j = 0$. The result is

$$\begin{aligned} T'_{kl} &= T_{k,l+1} + \tau_{k-1}\sigma_k T_{k+1,l+1} \\ &= (\tau_k + \tau_{k-1}\sigma_k) T_{k+1,l+1} \\ S'_{kl} &= S_{k-1,l} + S_{k-1,l-1}\tau_l \sigma_{l+1} \\ &= S_{k-1,l-1}(\sigma_l + \tau_l \sigma_{l+1}). \end{aligned} \tag{11}$$

Multiplication of both equations in (11) then gives

$$(T_{kn} S_{n+1,l})' = (\tau_k + \tau_{k-1}\sigma_k) T_{k+1,n+1} S_{n,l-1}(\sigma_l + \tau_l \sigma_{l+1}) = 0 \tag{12}$$

where the relation $\tau_n \sigma_n = 0$ has been used.

The implications of (12) are quite interesting, as it states that a configuration containing $(\ldots 1100 \ldots)$ *cannot* be created. As all possible configurations have evolved from the empty initial state, configurations containing a cluster of particles *tailing* a cluster of holes on its r.n.n. site do not exist in the NESS.

Moreover, a configuration $(\ldots 110100 \ldots)$ with a single particle–hole pair separating the two clusters cannot be created either. The reason is that only the nonexistent configuration $(\ldots ?1100? \ldots)$ in the previous timestep could have created the configuration under consideration. The question mark represents a '0' or a '1'.

Similarly a configuration $(\ldots 11(01)^k 00 \ldots)$ with k $(k = 1, 2, 3, \ldots)$ intermediate hole–particle pairs does not exist, as it could only have been created from the configuration $(\ldots ?1(10)^k 0? \ldots) = (\ldots ?11(01)^{k-1}00? \ldots)$. It then follows by complete induction that none of the above configurations can exist in the NESS.

Consequently, the possible configurations generated by the dynamics from the empty initial state do not contain any configurations with two or more empty sites to the right of the left most cluster of particles. So, the fully parallel dynamics of the present TASEP builds up very strong short-range correlations in the NESS.

From the observations about the build up of dynamic correlations, we arrive at some important conclusions about the structure of the NESS. Let k_0 label the position of the left-most particle in the left-most particle cluster†. The configurations in the interval $[1, k_0 - 1]$ consist of *isolated* particles, separated by an arbitrary number of holes. In these so-called *free-flow* configurations

$$\tau_{i-1}\tau_i = 0 \qquad (i < k_0) \tag{13}$$

i.e. there is a 'hard core repulsion' between particles on *nearest-neighbour* sites. The instantaneous fraction of occupied sites (density) in this interval is therefore $\rho(< k_0) < \frac{1}{2}$. The configurations in the interval $[k_0, L]$ consist of *isolated* holes, separated by an arbitrary number of particles. In these so-called *jammed* configurations

$$\sigma_{i-1}\sigma_i = 0 \qquad (i > k_0) \tag{14}$$

i.e. there is a 'hard core repulsion' between holes on nearest-neighbour sites. The instantaneous fraction of occupied sites in this interval $\rho(> k_0) > \frac{1}{2}$.

Therefore, *large* systems with an overall density (fraction of occupied sites) $\rho < \frac{1}{2}$ necessarily have only bulk configurations of the free-flow type with a narrow *boundary layer* of jammed configurations near the exit site of (yet unknown) width $\lambda_R << L$, whereas for $\rho > \frac{1}{2}$ bulk sites contain only jammed configurations with a narrow boundary

† Note, however, that an instantaneous configuration of the whole system may not contain any cluster of particles (at low densities) or any clusters of holes (at high densities).

layer of free-flow configurations of width λ_L near the entrance site. Which value of ρ occurs, depends on the injection and removal rates, α and β, and will be determined in section 4.1, where *averages* will be considered.

3.2. Instantaneous profiles

To study the density profile we consider the creation of pairs and larger clusters from a purely dynamical point of view. We first observe that the first particle pair can only be created *at* the exit site and only if $\beta < 1$. This follows from the evolution equation (11) for $T_{k,k+1}$ which shows that the creation of a new pair at $(k, k+1)$ requires the existence of a pair at $(k+1, k+2)$. Therefore, creation of the *first* pair $T_{L-1,L}$ at $t+1$ is governed by

$$(\tau_{L-1}\tau_L)' = (\tau_{L-1} + \tau_{L-2}\sigma_{L-1})\tau_L(1-\hat{\beta}) \tag{15}$$

where the term $\tau_{L-1}(t)\tau_L(t)$ on the right-hand side of the equation vanishes, as this pair has not yet been created. This implies that pairs cannot be created if $\langle\hat{\beta}\rangle = \beta = 1$. Consequently, if $\beta = 1$, there is no boundary layer near the exit, the density profile is totally *flat* over the whole system and all configurations are pure free-flow configurations. All space- and time-dependent correlations in this NESS can be calculated exactly in a simple manner, as will be shown in section 5.2, where spatial and temporal *correlations* will be studied.

If $\beta < 1$, however, particle clusters can be created near the exit site. In the case in which the injection rate is smaller than the removal rate, the average interval between arrivals $1/\alpha$ at the pile-up region near the exit is larger than the average interval $1/\beta$ between removals, and a large fraction of configurations are pure free-flow configurations without any clusters near the exit site. On average there is only a narrow boundary layer of jammed configurations. So, the bulk properties of the system in the low-density case $\alpha < \beta$ are determined by the injection rate α at the entrance site.

In the jammed phase ($\alpha > \beta$), there is on average a large backup starting near the exit and extending to the left. The jammed configurations in the NESS cover the bulk of the system, leaving only a narrow boundary layer with free-flow configurations near the entrance. The bulk properties in the high-density phase are determined by the removal rate β at the exit site. We also note that the phase diagram of the stochastic model of [8] contains a line $(1-\alpha)(1-\beta) = 1-p$, where the density profile is *flat* over the whole system. In the present deterministic model ($p = 1$) this corresponds to the line $\beta = 1$ (free-flow phase), and to the line $\alpha = 1$ (jammed phase).

4. Phase diagram

4.1. Free-flow and jammed phases

For large system size L (thermodynamic limit) and $\alpha < \beta$ the system is in the free-flow phase, and the dynamics rigorously implies that the bulk of the system (except the boundary layer near the exit) has only *isolated* particles. So, in the thermodynamic limit, this low-density phase is characterized by an average density (occupation) $\rho < \frac{1}{2}$ and has the *vanishing* order parameters $\langle\tau_i\tau_{i+1}\rangle = \langle\tau_i\tau_{i+1}\tau_{i+2}\rangle = \cdots = 0$ when i is a *bulk site*, defined as $i << L - \lambda_R$ with λ_R the width of the boundary layer near the exit. In fact, even the microscopic order parameter $\tau_i\tau_{i+1} = 0$ in the free-flow phase on the basis of (13). Of course the correlations $\langle\sigma_i\sigma_{i+1}\rangle$, $\langle\sigma_i\sigma_{i+1}\sigma_{i+2}\rangle$ etc, are *nonvanishing* in this phase.

Moreover, the vanishing order parameter $\langle \tau_i \tau_{i+1} \rangle = 0$ for bulk sites, in combination with relations (5) imply the following properties of the low-density *free-flow* phase:

$$\begin{aligned} & j = \langle \tau_1 \rangle = \langle \tau_2 \rangle = \cdots = \langle \tau_i \rangle = \rho \\ & \langle \tau_1 \rangle = j = \rho = \alpha/(1+\alpha) \\ & \langle \tau_L \rangle = j/\beta = \alpha/[\beta(1+\alpha)] \end{aligned} \tag{16}$$

where the *bulk density* ρ is defined as the average occupation $\langle \tau_i \rangle$ at a bulk site i. Because there is an excess density in the right boundary layer, the bulk density $\rho = \langle N \rangle / L - |\mathcal{O}(\lambda_R/L)|$ in the low-density phase, where $\langle N \rangle = \sum_{i=1}^{L} \langle \tau_i \rangle$.

Several interesting features can be seen. First of all, the bulk dynamics is completely determined by the input rate α at the entrance site, as already explained in section 3.2. Second, the flux equals the bulk density, indicating that particles are never blocked in the free-flow phase, and are travelling with an average speed $v_F \equiv j/\langle \tau_i \rangle = 1$. A particle entering the lattice is never blocked until it leaves the bulk and enters the boundary layer near the exit, where it slows down to a velocity $v_J = j/\langle \tau_L \rangle = \beta$ with $\beta < 1$ as a consequence of the pile up. The bulk density of the system, $\rho = \alpha/(1+\alpha)$, is always smaller than $\frac{1}{2}$, since $\alpha < \beta \leqslant 1$. Therefore, we will also refer to the phase with $\alpha < \beta$ as the *low-density phase* of the system.

Similarly there is in the thermodynamic limit a *jammed* phase for $\alpha > \beta$ of high density $\rho > \frac{1}{2}$, containing only isolated holes except in a boundary layer of width λ_L near the entrance where there is a deficit density in comparison with the bulk density. The phase is characterized by the microscopic order parameter $\sigma_i \sigma_{i+1} = 0$, or equivalently by the nonvanishing order parameters $\langle \tau_i \tau_{i+1} \rangle$, $\langle \tau_i \tau_{i+1} \tau_{i+2} \rangle$, etc, in the bulk.

The properties of the high-density phase with $\alpha > \beta$ can be related to those of the low-density phase with $\alpha < \beta$ by the particle–hole symmetry of section 2.2. In this case, particle–hole symmetry implies that the dynamics of particles moving forward is identical to that of the holes moving backwards. In this point of view holes are injected at the exit site with probability β and move downstream where they are finally removed from the lattice with probability α. So, (16) implies for the *jammed* phase:

$$\begin{aligned} & \rho = \langle \tau_L \rangle(\alpha, \beta) = \langle \sigma_1 \rangle(\beta, \alpha) \\ & \quad = 1 - \langle \tau_1 \rangle(\beta, \alpha) = 1/(1+\beta) \\ & \langle \tau_L \rangle = \langle \tau_{L-1} \rangle = \cdots = \langle \tau_i \rangle = \rho \\ & \langle \tau_1 \rangle(\alpha, \beta) = 1 - \langle \tau_L \rangle(\beta, \alpha) = 1 - \beta/[\alpha(1+\beta)] \end{aligned} \tag{17}$$

where i is a bulk site in the jammed phase, defined as $i >> \lambda_L$. Similarly the average flux in the jammed phase follows from (9) as

$$j = j_J(\alpha, \beta) = j_F(\beta, \alpha) = \frac{\beta}{1+\beta} = \beta\rho = 1 - \rho \tag{18}$$

which implies an average speed $v_J \equiv j/\rho = \beta$. In the boundary layer near the entrance a particle has a higher average speed, $v_1 = j/\langle \tau_1 \rangle$, and it slows down to speed β, because of frequent blockage by a preceding particle. The average flux may also be written as $j = 1 - \rho$, indicating that the flux in the jammed phase equals the density of holes, which move with unit speed to the left. We note that these results are exact in the thermodynamic limit as $L \to \infty$.

It is interesting to compare the results (16)–(18) for fully parallel updating with those for *sublattice–parallel* updating, as derived in (A5)–(A7) of the appendix. Let $\langle \tau_+ \rangle$ and $\langle j_+ \rangle$ be respectively the bulk density and the flux at even sites, as defined in the appendix, and

$\langle j_- \rangle$ and $\langle \tau_- \rangle$ the corresponding ones for odd sites, then we have for the sublattice–parallel dynamics in the *free-flow* phase ($\alpha < \beta$),

$$\begin{aligned} &\langle \tau_+ \rangle = \alpha \qquad \langle \tau_- \rangle = 0 \qquad \langle \tau_L \rangle = \alpha/\beta \\ &\langle j_+ \rangle = \alpha \qquad \langle j_- \rangle = 0 \end{aligned} \tag{19}$$

and for the *jammed* phase ($\alpha > \beta$)

$$\begin{aligned} &\langle \tau_+ \rangle = 1 \qquad \langle \tau_- \rangle = 1 - \beta \qquad \langle \tau_1 \rangle = 1 - \beta/\alpha \\ &\langle j_+ \rangle = \beta \qquad \langle j_- \rangle = 0. \end{aligned} \tag{20}$$

The average properties, in particular of the odd sites, are very different from the TASEP with fully synchronous dynamics.

Before concluding this section we discuss the collective dynamics in the different bulk phases. In the low-density or free-flow phase every particle has at least one hole to its right. Consequently it will advance one site per timestep, and has the maximum speed $v_F = 1$. In fact any free-flow configuration with a hole to its right is propagated as a whole with velocity $v_F = 1$. In the jammed phase on the other hand, every cluster of c particles is preceded by a single hole. At every timestep *only* the lead particle of each cluster advances one site, and becomes the tail particle of the preceding cluster. Therefore clusters of constant length are moving backwards with unit speed, and so do isolated holes. The cth particle in a cluster makes its first move only after c timesteps, and the average speed of a particle $v_J = \beta$ (see (18)). The motion in the jammed phase is therefore characterized by *start–stop waves*, which are typical for congested traffic flows.

4.2. Coexisting phases

From the analysis of the dynamics of section 3.2 we can also infer some properties for the case $\alpha = \beta$. Then there exist on the left-hand side of the system free-flow configurations (low-density phase) and on the right side jammed configurations (high-density phase). Each of them occupies a finite fraction of the system. The two *coexisting phases* are separated by an interface of microscopic width which contains only particle–hole pairs.

When $\alpha \uparrow \beta$, the bulk density $\rho = \alpha/(1+\alpha)$ in the free-flow (low density) phase increases untill it reaches its value $\rho_F = \alpha/(1+\alpha) = \beta/(1+\beta)$ at *coexistence*. At the same time the right boundary layer λ_R grows to a region of macroscopic size, containing the jammed phase. In the jammed (high-density) phase, the density $\rho = 1/(1+\beta)$ is controlled by the release rate β. As $\beta \downarrow \alpha$ the bulk density also grows to its coexistence value $\rho_J = 1/(1+\beta) = 1/(1+\alpha)$.

In open systems at coexistence ($\alpha = \beta$) the instantaneous position R of the interface wildly fluctuates, as it can be anywhere on the lattice with uniform probability. For a system of $L = 1000$ sites this statement has been verified by collecting 1.2×10^7 measured values of R into 10 equal-sized bins. The resulting histogram is flat within fluctuations of 1%.

Consequently, for $\alpha = \beta$ the *instantaneous* overall density, $\hat{\rho} \equiv (1/L)\sum_i \tau_i$, fluctuates between $\rho_F = \alpha/(1+\alpha)$ and $\rho_J = 1/(1+\alpha)$. For *large* systems (in the approximation of zero interface width), the instantaneous density is given by

$$\hat{\rho} = \hat{\rho}(R) = \frac{R}{L}\frac{\alpha}{1+\alpha} + \left(1 - \frac{R}{L}\right)\frac{1}{1+\alpha}. \tag{21}$$

The average density $\rho = \langle \hat{\rho}(R) \rangle$ with R uniformly distributed over the system yields $\langle R \rangle = \frac{1}{2}L$ and $\rho = \frac{1}{2}$, in agreement with the *exact* result to be derived in (49). Moreover, we calculate the expected density $\rho(x)$ at site x, by averaging the instantaneous profile,

$\hat{\rho}(x|R) = \rho_F\theta(R-x) + \rho_J\theta(x-R)$, over R, where $\theta(x)$ is the unit step function. This yields the *linear* density profile,

$$\rho(x) = \frac{1}{L}\sum_{R=1}^{L}\hat{\rho}(x|R) = \rho_F\left(1-\frac{x}{L}\right) + \rho_J\frac{x}{L}. \tag{22}$$

In the *exact* results of [11–13] for the TASEP with sublattice–parallel updating also a linear form for the average density profile at coexistence has been found.

Of course, the instantaneous density profile $\hat{\rho}$ does not have a zero width as assumed in (21), but a finite one, as will be discussed now by studying the dynamics of the interface. To define the instantaneous location R and the instantaneous width w of the interface we introduce its front and tail sites l_0 and j_0. Let j_0 be the position of the right-most hole in the right-most cluster of holes, and l_0 that of the left-most particle in the left-most cluster of particles, where $j_0 < l_0$ (see section 3.1). The sites j_0 and ℓ_0 belong with certainty to the low- and high-density phase respectively. Then the interval $(j_0, \ell_0 = j_0 + 2n + 1)$ contains only n alternating particle–hole pairs $(10)^n$ $(n = 0, 1, 2, \ldots)$, which are allowed in both phases. The instantaneous position of the interface is defined as $R = \frac{1}{2}(j_0 + l_0)$ and its instantaneous *width* as $w(n) = 2n = l_0 - j_0 - 1$. As the particle (hole) cluster is moving with unit speed forward (backward), the width decreases by 2 units per timestep, vanishing after n times steps and yielding a hole cluster adjacent to the particle cluster. During this period $R = \frac{1}{2}(j_0 + \ell_0)$ remains fixed.

What happens next depends on the sizes h and c of the two adjacent hole and particle clusters respectively. If $h > c$, the positions j_0 and l_0 remain fixed during $(h-2)$ timesteps. After $(h-1)$ timesteps the cluster of particles disappears, and j_0 moves one site forward, whereas l_0 makes a forward *jump* to the right-most particle on the then right-most cluster. If $h < c$, the same statements can be make with l_0/c/particles/forward interchanged with j_0/h/holes/backwards respectively. If $c = h$ both points j_0 and l_0 *jump simultaneously*. The dynamics of the interface width is illustrated in figure 1.

The probability distribution of the sizes of the right and left jumps, as well as those for the time intervals between the jumps, are determined by the probability distribution of finding n particle–hole pairs between two particle clusters in the high-density region, or between two hole clusters in the low-density region. The position R of the interface performs a random walk over all sites of the system around the average position $\langle R\rangle = L/2$. Once the above probability has been calculated, its mean-square displacement $(\delta R)^2 = \langle(R - L/2)^2\rangle$ and the associated short time diffusion coefficient $\mathcal{D}$ can be calculated in principle for time intervals T satisfying the inequality $\delta R = \sqrt{2\mathcal{D}T} \ll L/2$. The long time diffusion coefficients vanishes due to the presence of the boundaries. Here we only illustrate the basic idea of the method by calculating the average width $\langle w\rangle$ of the interface, using a mean-field estimate.

The width $\langle w\rangle$, measured over a long time interval, is shown in figure 2, as a function of the injection rate. This behaviour can be understood on the basis of simple arguments. Let the instantaneous interface configuration be $(\ldots?00(10)^n11?\ldots)$ with $(n = 0, 1, 2, \ldots)$, then its width is $w(n) = 2n$. The probability on the configuration $(00(10)^n)$ tailing $(11?\ldots)$—which is the start of the jammed phase—is $P(n) = (1-\alpha)\alpha^n$, where α^n is the probability for injecting n particles and $(1-\alpha)$ the probability for not injecting a particle. In the present asymmetric exclusion process, every injected particle is followed by a hole. The average interface width is then

$$\langle w\rangle = \sum_n 2nP(n) = 2/(1-\alpha). \tag{23}$$

This estimate gives a good representation of the simulation results, as shown in figure 2.

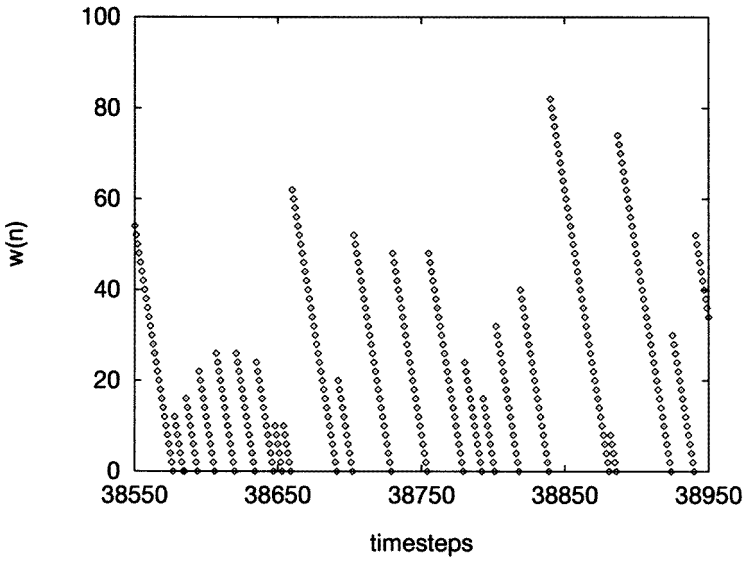

Figure 1. Instantaneous interface width w between coexisting phases as a function of time, measured for $L = 1000$, $\alpha = \beta = 0.9$. Notice the saw-tooth behaviour of the width, corresponding to right and/or left jumps of the interface boundaries.

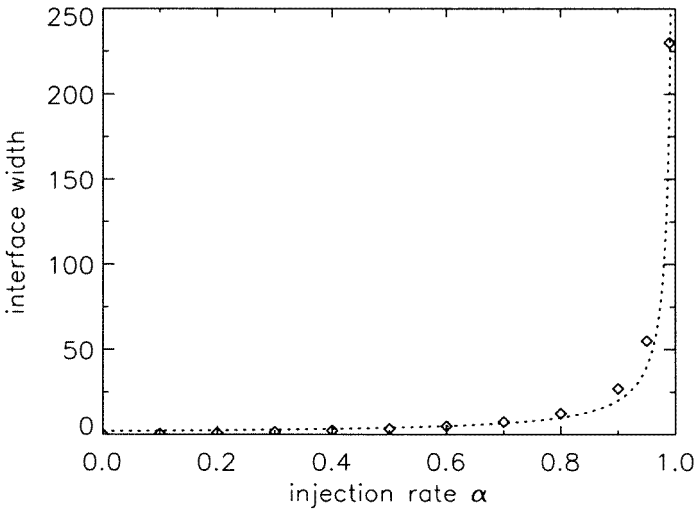

Figure 2. Average interface width $\langle w \rangle$ between coexisting phases, measured over an interval of 2×10^4 timesteps, as a function of injection rate α, in a system with $L = 1000$, and compared with the theoretical prediction $\langle w \rangle = 2/(1-\alpha)$. As $\alpha \uparrow 1$, the width of the interface changes from microscopic to macroscopic.

4.3. Equation of state $j(\rho)$

The results of sections 4.1 and 4.2 allow us to construct the flux $j(\rho)$ as a function of the bulk density ρ, as shown in figure 3. It is the analogue of the equation of state for the pressure in thermal equilibrium.

In the low-density phase ($\rho < \rho_F$), the density $\rho = \alpha/(1+\alpha)$ varies as α runs in the

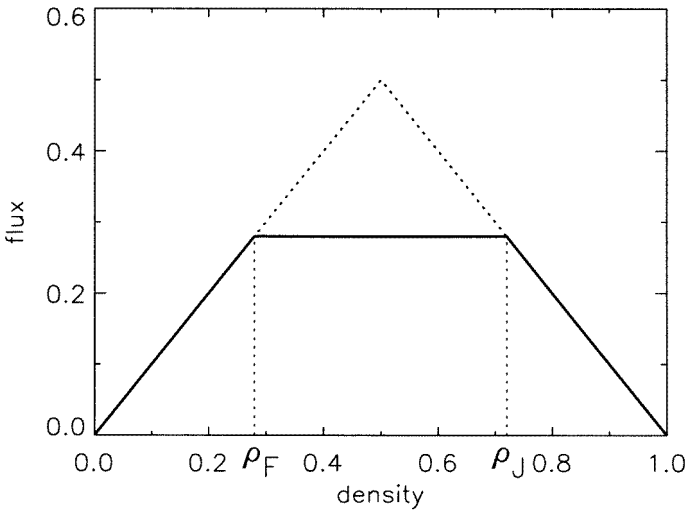

Figure 3. Flux $j(\rho)$ as a function of density ρ (full curve). For $\rho < \rho_F$ the flux is $j = \rho$, and for $\rho > \rho_J$ it is $j = 1-\rho$. For $\rho_F < \rho < \rho_J$ with $\rho_F = \beta/(1+\beta)$ and $\rho_J = 1/(1+\beta)$ the flux $j = \rho_F$ remains constant. The triangle bounding the region $j < \min\{\rho, 1-\rho\}$ of coexisting phases is called the fundamental diagram in traffic flow problems.

interval $(0, \beta)$ with β kept fixed, and the flux $j(\rho) = \rho$ increases to its coexistence value $\rho_F = \beta/(1+\beta)$ as $\alpha \uparrow \beta$.

In the high-density region ($\rho_J < \rho < 1$), the density, $\rho = 1/(1+\beta)$, can be varied by keeping α fixed, and taking $\alpha < \beta < 1$. The flux is given by $j(\rho) = 1 - \rho$.

Let us compare the behaviour of flux j and bulk density ρ when crossing the transition line $\alpha = \beta$, where $\rho = \alpha/(1+\alpha)$ and $j = \rho$ in the low-density phase, and $\rho = 1/(1+\beta)$ and $j = 1-\rho$ in the high-density phase. This shows that the flux j is continuous across the line $\alpha = \beta$, whereas the density makes a jump $\triangle\rho = \rho_J - \rho_F = (1-\alpha)/(1+\alpha)$. Therefore the NESS of this model shows a first-order phase transition across the line $\alpha = \beta$. At coexistence ($\alpha = \beta$), the flux remains constant and the instantaneous overall density $\hat{\rho}$ fluctuates between ρ_F and ρ_J.

The triangle bounding the region ($j < \min\rho, 1-\rho$) is called the *fundamental diagram* in traffic problems, and corresponds to the coexistence region in thermodynamic phase transitions.

It should be remarked that the basic formula (21) in this section for the instantaneous density $\hat{\rho}(R)$ is simply the analytical representation of the conclusions of the dynamical analysis of sections 3.1 and 3.2, which fixes the values of the coexisting densities. In addition, there is an *a posteriori* justification of this formula through (23), which shows that the width of the *instantaneous* interface is of microscopic size for α not close to 1.

The uniform distribution, postulated for the position R of the interface, is only an observation deduced from computer simulations. Consequently, the average linear profile in (22) is a phenomenological result.

5. Correlation functions

5.1. Profiles and nearest-neighbour correlations

Consider first the low-density or free-flow phase where $\alpha < \beta$. To determine the density profile $\langle \tau_k \rangle$ from (6) we need the nearest-neighbour correlation function $\langle \tau_k \tau_{k+1} \rangle$, which represents the probability of finding the sites $(k, k+1)$ occupied. As already derived in section 4.1, we have $\langle \tau_k \rangle = \rho$ and $\langle \tau_k \tau_{k+1} \rangle = 0$ for *bulk* sites ($k \ll L - \lambda_R$). It remains to calculate these quantities in the boundary layer $k \gtrsim L - \lambda_R$ near the exit. To do so, we need the dynamics (11) of the cluster correlation functions (10), averaged over the NESS, where $\langle T' \rangle = \langle T \rangle$. This yields

$$\langle T_{k\ell} \rangle = \langle T_{k,\ell+1} \rangle + \langle \tau_{k-1} \sigma_k T_{k+1,\ell+1} \rangle \tag{24}$$

where $\ell = k+1, \ldots, L$ and we recall that $\tau_{L+1} = 1 - \hat{\beta}$. If $T_{k+1,\ell+1}$ refers to the left-most particle cluster, then the sites $(k-1, k)$ belong by definition to the boundary layer, and the probability of the configuration $\tau_{k-1}\sigma_k T_{k+1,\ell+1}$ equals α times the probability for the configuration $T_{k+1,\ell+1}$. Since $k+1$ is by definition the left-most site on the left-most particle cluster, the occupation number σ_k equals unity with probability 1. In fact there are only very few particle clusters in the pile-up region near the exit site, as the average removal interval $1/\beta$ is less than the average arrival interval $1/\alpha$ at the pile-up region. So, we expect that the least advanced particle cluster gives the dominant contribution to the probabilities, and we make the *mean-field assumption* that the above factorization holds for all further advanced particle clusters as well, i.e.

$$\langle T_{kl} \rangle = \langle T_{k,l+1} \rangle + \alpha \langle T_{k+1,l+1} \rangle. \tag{25}$$

The present MFA therefore assumes that four-point correlations and higher-order ones between a particle–hole pair and the particle cluster just on its r.n.n. site (which by definition belong to the boundary layer in the present model) are negligible in the low-density phase.

The recursion relation above can be solved starting from $l = L$, where $\langle T_{k,L+1} \rangle = \langle T_{kL} \rangle (1-\beta)$, and yields after iteration

$$\langle T_{kL} \rangle = \frac{\alpha(1-\beta)}{\beta} \langle T_{k+1,L} \rangle = \left(\frac{\alpha(1-\beta)}{\beta} \right)^{L-k} \langle \tau_L \rangle \tag{26}$$

where we have used the relation $\langle T_{L,L} \rangle = \langle \tau_L \rangle$. Taking $\ell = L-1, L-2$, etc gives $\langle T_{k,L-1} \rangle = (\alpha/\beta) \langle T_{k+1,2} \rangle$, etc and one finds by complete induction

$$\langle T_{k,L-\ell} \rangle = \left(\frac{\alpha}{\beta} \right)^{l} \langle T_{k+l,L} \rangle. \tag{27}$$

Combining this with (26) yields

$$\langle T_{k\ell} \rangle = \langle \tau_k \tau_{k+1} \ldots \tau_l \rangle = \left(\frac{\alpha}{\beta} \right)^{L-k} (1-\beta)^{l-k} \langle \tau_L \rangle. \tag{28}$$

The density profile is then obtained by inserting (28) for $l = k+1$ in (6) with the result

$$\langle \tau_k \rangle = j \left\{ 1 + \frac{1-\beta}{\beta} \left(\frac{\alpha}{\beta} \right)^{L-k} \right\} \tag{29}$$

where $\langle \tau_L \rangle = j/\beta = \alpha/[\beta(1+\alpha)]$ has been used. By taking the thermodynamic limit of (28) and (29) one recovers the properties of sections 3 and 4 for the bulk phase, i.e. the order parameters $\langle \tau_k \tau_{k+1} \rangle = \langle \tau_k \tau_{k+1} \tau_{k+2}, \ldots \rangle$ are vanishing, and the bulk density is $\rho = \langle \tau_k \rangle = j$. In addition (29) describes the profile of the *boundary layer* near the exit. The excess density,

which equals the nearest-neighbour correlation $\langle \tau_k \tau_{k+1} \rangle$, decreases exponentially on a length scale $1/\ln(\beta/\alpha)$, *independent* of the system size.

Our mean-field assumption, formulated first above (25), also implies that site k in T_{kl} marks the beginning of the boundary layer. Hence, the probability $P(k)$ that the width of the boundary layer is $L-k$, is then *proportional* to the excess density $\langle \tau_i \rangle - j$ in (29), yielding after proper normalization,

$$P(k) = \zeta^{L-k}/(1-\zeta) \tag{30}$$

with

$$\zeta = \alpha/\beta. \tag{31}$$

The expected width of the boundary layer in the low-density phase is then,

$$\lambda_B = \langle L-k \rangle = \frac{\zeta}{1-\zeta} = \frac{\alpha}{\beta-\alpha} \tag{32}$$

and the fluctuation $\delta\lambda_B$ around this average is

$$(\delta\lambda_B)^2 = \langle (L-k)^2 \rangle - \langle L-k \rangle^2 = \frac{\zeta}{(1-\zeta)^2} = \frac{\alpha\beta}{(\beta-\alpha)^2}. \tag{33}$$

The width of the boundary layer is 'microscopic' in nature, i.e. independent of the system size. In the limiting case as $\alpha \uparrow \beta$ (coexisting phases) the width λ_B diverges and becomes of macroscopic size. It is given by $L-R$, as the location R hops around over all sites of the lattice.

The correlation functions in the high-density or jammed phase with $\alpha > \beta$ can be obtained from particle–hole symmetry, for example $\langle \tau_k \tau_{k+1} \rangle(\alpha,\beta) = \langle \sigma_{L-k} \sigma_{L-k+1} \rangle(\beta,\alpha)$ and yields

$$\langle \tau_k \tau_{k+1} \rangle = \frac{1-\beta}{1+\beta} - \frac{1-\alpha}{1+\beta}\left(\frac{\beta}{\alpha}\right)^i. \tag{34}$$

Similarly, the density profile follows from (34) and (6) as

$$\langle \tau_k \rangle = \frac{1}{1+\beta}\left[1-(1-\alpha)\left(\frac{\beta}{\alpha}\right)^k\right]. \tag{35}$$

It shows a boundary layer near the entrance site with a deficit density that decays on a length scale $1/\ln(\alpha/\beta)$.

For the coexisting phase region, where $\alpha = \beta$, the boundary layers at both ends diverge, i.e. become of macroscopic size, and the typical width ξ of the interface $\xi = \langle w \rangle = 2/(1-\alpha)$, or equivalently $\sim 1/|\ln\alpha|$, as was calculated in section 4 on the basis of dynamical considerations.

In figure 4(a) the density profiles are compared with computer simulations, for two different combinations of parameter sets $\{\alpha = 0.50; \beta = 1\}$ and $\{\alpha = 0.50; \beta = 0.51\}$ and the results are *indistinguishable*. For $\beta = 1$ the profile is flat, as already explained in the first paragraph of section 3.2. Moreover we have compared simulations and theoretical predictions for the three- and four-point correlation functions $\langle \tau_k \tau_{k+1} \tau_{k+2} \ldots \rangle$ for $\alpha = 0.50$ and $\beta = 0.55$. The former ones are shown in figure 4(b), and the results are again indistinguishable.

In the appendix the density profile and correlation functions for the same TASEP with sublattice–parallel updating [11] have been calculated, using the same mean-field theory.

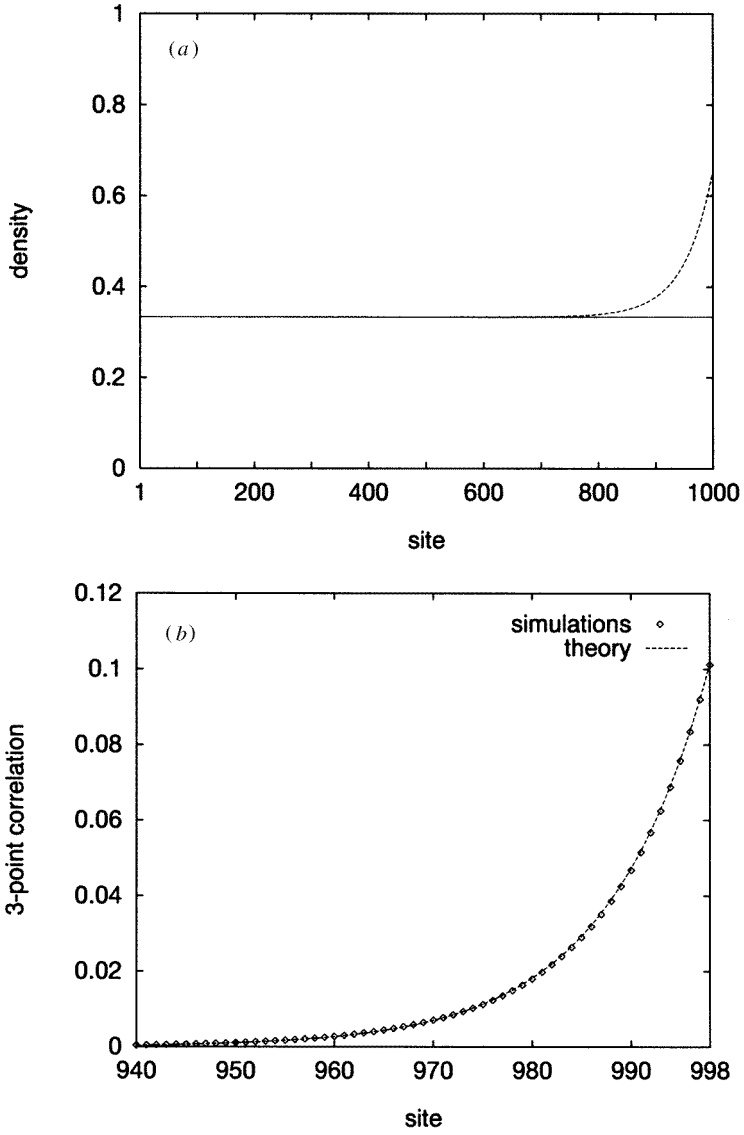

Figure 4. (*a*) Density profiles for $\{\alpha = 0.50; \beta = 1\}$ (full curve) and $\{\alpha = 0.50; \beta = 0.51\}$ (broken curve) for a system with $L = 1000$. The bulk densities are the same (see (16)), except in the boundary layer, where the excess density is $\langle \tau_i \tau_{i+1} \rangle$, averaged over 1.3×10^7 timesteps. (*b*) the three-point correlation $\langle \tau_i \tau_{i+1} \tau_{i+2} \rangle$. In both plots the theoretical (broken curve) and simulation results (diamonds) are indistinguishable. The latter are time averaged over 1.8×10^4 timesteps.

Here the average flux is quite different, i.e. $j = \beta \langle \tau_L \rangle = \alpha$, but the profile $\langle \tau_k \rangle / j$ is quite similar, i.e.

$$\langle \tau_k \rangle = j \left\{ \delta_{k,\text{even}} + \frac{1-\beta}{\beta} \left(\frac{\alpha}{\beta} \right)^{L-k} \right\} \tag{36}$$

at least for even sites. For comparison we also quote the results for the correlation functions, as derived in (A11) of the appendix, i.e.

$$\begin{aligned}\langle T_{kl}\rangle &= \langle T_{k,l-1}\rangle = \frac{\alpha}{\beta}\langle T_{k+1,l}\rangle = \frac{\alpha}{\beta}\langle T_{k+1,l-1}\rangle \\ &= \left(\frac{\alpha}{\beta}\right)^{L-k}(1-\beta)^{\frac{1}{2}(l-k)}\langle \tau_L\rangle \end{aligned} \tag{37}$$

which should be compared with (28). We emphasize that k, l and L are *even* numbers in the present formulae. Comparison with (28) shows that the correlation functions are quite different, in particular the differences between *even* and *odd* sites. The results (36) and (37) are *exact* to terms of order $(\alpha/\beta)^L$, as can be verified by comparison with the exact results derived in [11, 13].

We *conjecture* that the corresponding results (26)–(35) for the same TASEP with fully parallel updating and with open boundaries are also exact, up to exponential terms of order $(\alpha/\beta)^L$ for $\alpha < \beta$, and up to $(\beta/\alpha)^L$ for $\alpha > \beta$. However, for α close to β, say $\alpha = \beta(1-\delta/L)$, the expressions for the profiles in the boundary layers break down, as the neglected terms $(\alpha/\beta)^L \simeq \exp(-\delta)$ become of $\mathcal{O}(1)$ for large L.

5.2. Spatial and Temporal Correlations

Next we will determine the correlation functions $\langle \tau_i \tau_{i+x}\rangle$ for *bulk* sites in the low-density phase ($\alpha < \beta \leqslant 1$). As explained in section 4.1 the dynamics rigorously implies that the 'microscopic' order parameter $\tau_i\tau_{i+1} = 0$ in the bulk phase. Consequently, the microdynamic equation for all sites outside the pile-up region near the exit becomes

$$\begin{aligned}\tau_1' &= \tau_0\sigma_1 = \hat{\alpha}(1-\tau_1) \\ \tau_i' &= \tau_{i-1} \qquad (1 < i \ll L - \lambda_R).\end{aligned} \tag{38}$$

The last relation implies *translational invariance* of the correlation for the bulk phase, i.e.

$$\begin{aligned}\langle \tau_i\tau_{i+x}\rangle &= \langle \tau_{i-1}\tau_{i+x-1}\rangle = \cdots \\ &= \langle \tau_1\tau_{1+x}\rangle = \alpha\langle\tau_x\rangle - \alpha\langle\tau_1\tau_x\rangle.\end{aligned} \tag{39}$$

The last equality follows from (38) for τ_1. Then (39) implies that the pair distribution function, defined as $g(x) = \langle\tau_1\tau_{1+x}\rangle/\langle\tau_{1+x}\rangle$, satisfies the recursion relation

$$g(x+1) = \alpha - \alpha g(x). \tag{40}$$

We calculate the generating function, $F(x) \equiv \sum_{x=0}^{\infty} z^x g(x)$ where $g(0) = 1$, by multiplying (40) with z^{x+1} and summing over x. Solving this equation then yields

$$F(z) = \frac{1 - z(1-\alpha)}{(1+\alpha z)(1-z)}. \tag{41}$$

After decomposing the right-hand side of (41) into partial fractions, and expanding the result in powers of z, we find the pair correlation function in the bulk of the low-density phase:

$$g(x) = [\alpha + (-\alpha)^x]/(1-\alpha) \tag{42}$$

which yields

$$\begin{aligned}\langle \tau_i\tau_{i+x}\rangle &\equiv \langle\tau_i\rangle\langle\tau_{i+x}\rangle[1 + C(x)] \\ &= \langle\tau_1\rangle^2[1 - (-\alpha)^{x-1}].\end{aligned} \tag{43}$$

This is an asymptotically exact result for $1 \leqslant \{i, i+x\} \ll L - \lambda_R$. In the case in which $\beta = 1$ there is no right boundary layer, and (43) is exact for all interparticle distances

x. The pair function oscillates around its uncorrelated value, it vanishes for $R = 1$, as it should, and is independent of β, because the bulk phase is only determined by the injection rate α. Neighbour particles are strongly correlated. The spatial correlation function in the bulk $C(x) = -(-\alpha)^{x-1}$ decays exponentially with a correlation length $\xi_F = 1/|\ln\alpha|$. This correlation length becomes of macroscopic size as $\alpha \to 1$ and $\beta = 1$, where the system approaches the critical maximal current phase [9], which in the present model is only realized at the parameter values $\alpha = \beta = 1$.

The result (43) for the bulk correlations is very different from those in [11, 13] for sublattice–parallel dynamics, where the spatial correlations do not depend on the interparticle distance x. For instance, in that model one has in the *bulk* of the low-density phase

$$\langle \tau_i \tau_{i+x} \rangle = \begin{cases} \langle \tau_1 \rangle^2 (1+\alpha) & (i, x \text{ even}) \\ 0 & (\text{elsewhere}). \end{cases} \tag{44}$$

So far we have discussed spatial correlation functions for bulk sites of the NESS. Similar results can be obtained for *time*- and *space*-dependent correlation functions. It follows from the microdynamic equation (38) that in the low-density phase

$$\tau_{i+x}(t) = \tau_{i+x-1}(t-1) = \cdots = \tau_{i+x-t}(0) \tag{45}$$

and consequently we have the asymptotically exact result,

$$\begin{aligned} \langle \tau_{i+x}(t)\tau_i(0)\rangle &= \langle \tau_{i+x-t}\tau_i \rangle \\ &= \langle \tau_1 \rangle^2 \{1 - (-\alpha)^{x-t-1}\} \end{aligned} \tag{46}$$

valid for $0 \leqslant \{i, j\} \ll L - \lambda_R$ with $j = i + x - t$ and $x \neq t$. For the special case $\beta = 1$ the result (46) is exact for all sites and for all times.

One may also consider correlation functions involving fluxes. In the *low-density* phase ($\alpha < \beta$) we have

$$\langle \tau_{i+x}(t)\tau_i(0)\rangle = \langle \hat{\jmath}_{i+x}(t)\tau_i(0)\rangle = \langle \hat{\jmath}_{i+x}(t)\hat{\jmath}_i(0)\rangle \tag{47}$$

because the macroscopic order parameter $\tau_i \tau_{i+1} = 0$. The result obtained for the low-density phase can be easily extended to the *high-density* phase using particle–hole symmetry and the relation $\hat{\jmath} = \sigma_{i+1}$ on account of (3) and (14). This yields for bulk sites

$$\begin{aligned} \langle \tau_i \tau_{i+x}\rangle(\alpha,\beta) &= \langle 1 - \tau_{L-1+1} - \tau_{L-x-i+1} - \tau_{L-i+1}\tau_{L-x-i+1}\rangle(\beta,\alpha) \\ &= \frac{1}{(1+\beta)^2}\{1 - (-\beta)^{x+1}\} = \langle \tau_i \rangle^2 \{1 - (-\beta)^{x+1}\} \\ \langle \tau_i \hat{\jmath}_{i+x}\rangle(\alpha,\beta) &= \langle \tau_i \sigma_{i+x+1}\rangle(\alpha,\beta) \\ &= \langle \tau_{L-x-i}(1 - \tau_{L-i+1})\rangle(\beta,\alpha) \\ &= j\langle \tau_i \rangle \{1 - (-\beta)^{x+1}\} \\ \langle \hat{\jmath}_i \hat{\jmath}_{i+x}\rangle(\alpha,\beta) &= \langle \sigma_{i+1}\sigma_{i+x+1}\rangle = j^2\{1 - (-\beta)^{x-1}\}. \end{aligned} \tag{48}$$

For the *coexistence* region ($\alpha = \beta$) extensive measurements were made. It appears that the properties such as density, flux, etc, for both regions are equal to the properties in their associated phases. It seems interesting to measure the correlations between site i in the low-density region and site $i + x$ in the high-density region. However, due to the random nature of the interface location, the occupation numbers τ_i and τ_{i+x} appear to be uncorrelated, even if $x \leqslant 1/|\ln\alpha|$.

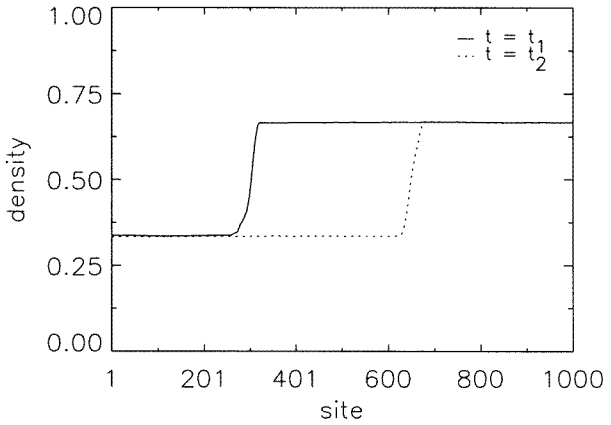

Figure 5. Density profiles in the coexistence region, time averaged over 4000 timesteps. At time t_1/t_2 the interface is at R is 302/649, and the average number of particles $\langle N\rangle$ is 566/450 respectively.

5.3. Profile on coexistence line

In section 3 the profile and interface between low- and high-density phase ($\alpha = \beta$) has been studied on the basis of purely dynamical considerations. A few additional results can be obtained from particle–hole symmetry (7) and the constant flux relation (5).

On the transition line $\alpha = \beta$, it follows from (8) that $\langle\tau_i\rangle = 1 - \langle\tau_{L-i+1}\rangle$. The density in the middle of the lattice is therefore on average $\frac{1}{2}$. The average number of particles $\langle N\rangle$ on the lattice follows by summing the above relation over all sites, and yields

$$\langle N\rangle = \sum_{i=1}^{L}\langle\tau_i\rangle = \tfrac{1}{2}L. \tag{49}$$

The flux $j = \alpha/(1+\alpha)$, which is continuous across the transition line (see section 3.1), allows us to calculate the boundary values exactly

$$\begin{aligned} &\langle\tau_1\rangle = \alpha/(1+\alpha) \qquad \langle\tau_L\rangle = 1/(1+\alpha) \\ &\langle\tau_1\tau_2\rangle = 0 \qquad \langle\sigma_L\sigma_{L-1}\rangle = 0. \end{aligned} \tag{50}$$

There are two coexisting phases, downstream of the interface the low-density phase with $\rho_F = \alpha/(1+\alpha)$ and upstream the high-density phase with $\rho_J = 1/(1+\alpha)$, separated by an interface located at R. This interface hops around over the whole lattice, where two instantaneous profiles (at t_1 and t_2) are shown in figure 5 for $\alpha = \beta = 0.50$.

5.4. Travel times

This section studies the travel time of the particles, which is by definition the number of timesteps that have passed from the moment a particle enters the lattice until it leaves the lattice. Because particles cannot travel with a speed larger than unity, the actual travel time will always be larger than or equal to the size of the lattice $T \geqslant L$. For the average travel time, the following definition is used:

$$\langle T\rangle = \sum_{i=1}^{L}\langle\tau_i\rangle/j = \langle N\rangle/j \tag{51}$$

where $\langle N \rangle$ denotes the average number of particles on the lattice. The resulting expression implies that the flux is equal to the average (unknown) number of particles $\langle N \rangle$ divided by the average travel time $\langle T \rangle$.

The present sections will give analytical and simulation results for travel times in low- and high-density phases, as well as travel times in the coexistence region. In the *low-density phase* of a large system ($L \to \infty$), the speed in the bulk equals unity. Therefore we expect the average travel time to be approximately equal to the size of the lattice, $\langle T \rangle \simeq L$. It can be calculated directly from (51) and the density profile in (29) and yields in the low-density phase ($\alpha < \beta$),

$$\begin{aligned} \langle T \rangle &= L + \frac{1-\beta}{\beta-\alpha}\left[1 - \left(\frac{\alpha}{\beta}\right)^L\right] \\ &= L + \frac{1-\beta}{\beta-\alpha} \qquad (L \to \infty). \end{aligned} \tag{52}$$

We observe that, for α and β not to close to one another, the travel times are of the order of L, as expected. Moreover, the average travel time $\langle T \rangle$ is a function of both parameters α and β. As $\alpha \uparrow \beta$, the neglected correction terms $(\alpha/\beta)^L$ in (52) and (29) become of $\mathcal{O}(1)$, and (52) is no longer valid.

For a large range of combinations of α and β, the average travel times have been measured with the simulation program, which is able to measure the travel times of a variable set of individual (labelled) particles. The measured travel times are in excellent agreement with relation (52), even very close to the transition line ($\alpha = \beta$). In figure 6(*a*) we show a histogram of travel times in a system with $L = 1000$, $\alpha = 0.50$, $\beta = 0.51$ in the low-density phase near the transition line $\alpha = \beta$, where travel times may vary considerably. The average travel time for the specific measurement was 1049 timesteps. Expression (52) gives $\langle T \rangle = 1049$, so the agreement is very good.

In the *high-density phase* ($\alpha > \beta$) the average travel time should be approximately L/β, because the speed in the bulk of the system is equal to $v_J = \beta$. The average travel time $\langle T \rangle$ can again be determined from definition (51) and (35) with the result

$$\langle T \rangle = \frac{L}{\beta} - \frac{1-\alpha}{\alpha-\beta} \qquad (L \to \infty). \tag{53}$$

For $\alpha = 1$ the average travel time assumes the value L/β. For $\alpha < 1$, the average travel time is smaller than L/β, because then the particles travel with a velocity larger than β just after entering the lattice. Comparison with the results of the low-density phase also show that the statistical spread in travel times is larger in the high-density phase, because the particles are often blocked by other particles. Figure 6(*b*) shows a histogram of the measured travel times for a lattice of $L = 1000$ sites, and injection and removal rates of $\alpha = 0.51$ and $\beta = 0.50$ respectively with a predicted average $\langle T \rangle = 1951$. Obviously there is a large spread around the average travel time (52). The distribution is not symmetric and therefore not a Gaussian. The asymmetry of the distributions in figures 6(*a*) and (*b*) are related through particle–hole symmetry.

The average travel time $\langle T \rangle$ on the transition line $\alpha = \beta$ can be easily determined, using the average number of particles in (51). The travel time combined with the flux $j = \alpha/(1+\alpha)$ then yields

$$\langle T \rangle = \langle N \rangle / j = \frac{1}{2} L \left(1 + \frac{1}{\alpha}\right). \tag{54}$$

This equation merely shows that in the coexistence region, the average travel time is just the average of the low- and high-density travel times, because both phases are present and

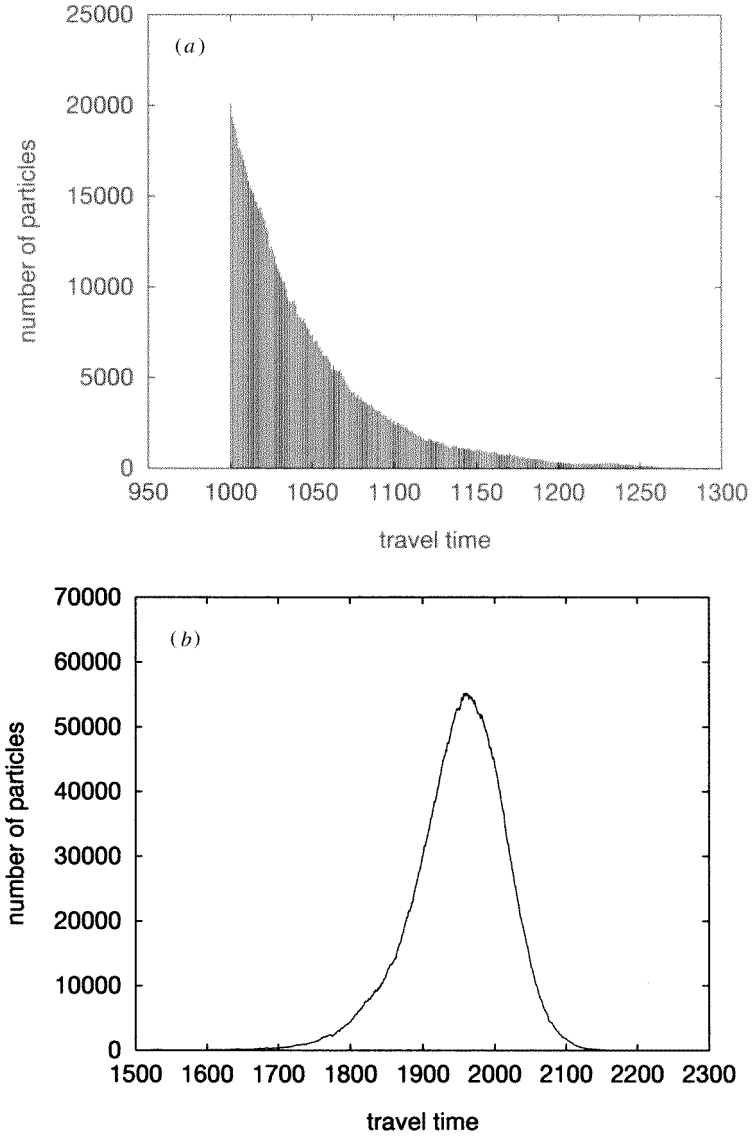

Figure 6. (*a*) Histogram of travel times for a system of $L = 1000$ in the low-density phase with $\{\alpha = 0.50; \beta = 0.51\}$ and (*b*) in the high-density phase with $\{\alpha = 0.51; \beta = 0.50\}$.

occupy on average an equal fraction of the system. The long-time average $\langle T \rangle$ agrees very well with (54). Individual particles will have a considerably shorter travel time of order L when R is located near the exit site, and a longer one of order L/α when R is located near the entrance site.

The prediction (54) is in excellent agreement with the simulation results, as shown in figure 7. We also note that the theoretical description of our totally asymmetric exclusion process in terms of occupation numbers (indistinguishable particles) does not allow us to calculate travel times of labelled particles, or calculate the probability distributions in

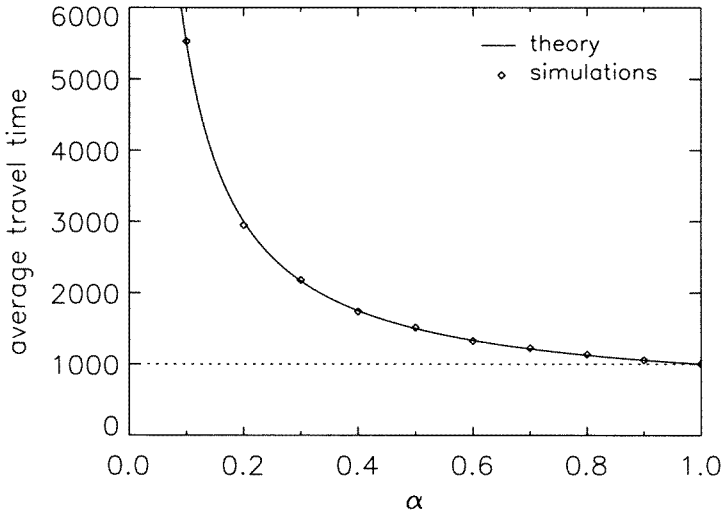

Figure 7. Average travel time $\langle T \rangle$ as a function of $\alpha = \beta$ for coexisting phases in a system with $L = 1000$ sites.

figure 6. Such calculations would only be possible in a TASEP with labelled particles, as considered in [17, 19].

6. TASEP on a ring with blockage site

The fully synchronous TASEP of section 2.1 as a closed system with $N = \rho L$ particles and obeying periodic boundary conditions is a fully deterministic, rather uninteresting system in its NESS. For $\rho < \frac{1}{2}$ all sites are in pure free-flow configurations and particles travel, say, counterclockwise with unit speed and flux $j = \rho$. For $\rho > \frac{1}{2}$ all sites are in jammed configurations, and holes are travelling clockwise with unit speed, and the flux $j = 1 - \rho$.

The dynamics becomes more interesting by inserting a stochastic blockage at site $i = L$ with a transmission rate $\beta < 1$. The microdynamic equation for sites $i = 2, 3, \ldots, L - 1$ is the same as in (1), (2), but the fluxes referring to the blockage sites are

$$\hat{j}_0 = \hat{j}_L = \hat{\beta}\tau_L\sigma_1 \tag{55}$$

where the Boolean variable $\hat{\beta}$ with expectation $\langle\hat{\beta}\rangle = \beta$, is defined in a similar manner as $\hat{\alpha}$ and $\hat{\beta}$ below (2). For $\beta = 1$ one recovers the fully deterministic case with periodic boundary conditions.

First we observe that the dynamics at *fixed* β is invariant under the duality transformation

$$\begin{aligned} &\tau_i \leftrightarrow \sigma_{L-i+1} \\ &\rho \leftrightarrow 1 - \rho \end{aligned} \tag{56}$$

and that the average occupation satisfies

$$\langle\tau_i\rangle(\rho, \beta) = \langle\sigma_{L-i+1}\rangle(1 - \rho, \beta). \tag{57}$$

A mean-field theory for the bulk properties of this model in the thermodynamic limit has already been given by Yukawa *et al* [21], as well as extensive numerical simulations, specially for the coexisting phase region. However, the correlation functions and density profiles have not yet been studied analytically. In the appendix we have discussed the TASEP

with open boundaries and sublattice–parallel updating. The corresponding models on a ring with a single blockage site and sublattice–parallel updating or with random sequential updating have also been solved exactly in [14–18]. However, the analytic results show little similarity with those for the present model, and will not be discussed further.

The build-up of dynamic correlations and structures may be analysed in a similar way as in section 3 for open systems, and one recovers (15), *except* for site $i = L$. This implies that a cluster of holes upstream of a particle cluster can only be created at the blockage site. Of course, hole clusters upstream of particle clusters may be present in the initial state anywhere on the lattice. In the low-density phase, such configurations will be destroyed in a time that is roughly equal to twice the size of the largest hole cluster. Moreover, from a detailed analysis of the dynamics, similar to section 3.1, one can derive exact relations for the microscopic dynamic correlations for the bulk of the low-density phase, such as

$$\begin{aligned} &\tau_i \tau_{i+1} = 0 \qquad \text{(bulksites } i \ll L - \lambda_B\text{)} \\ &\tau_L \tau_1 = 0 \qquad \text{(blockage site)} \end{aligned} \tag{58}$$

where λ_B is the width of the pile-up region, downstream of the blockage.

The continuity equation (1) and (55) yields then in combination with (58) for the low-density phase in the NESS,

$$\begin{aligned} j = \beta\langle\tau_L\rangle = \langle\tau_1\rangle = \langle\tau_2\rangle = \cdots = \langle\tau_i\rangle \qquad & (i \ll L - \lambda_B) \\ = \langle\tau_i\rangle - \langle\tau_i\tau_{i+1}\rangle \qquad & (L - \lambda_B \lesssim i < L). \end{aligned} \tag{59}$$

In the low-density phase there is an excess density in the pile-up region. Consequently, as the total density $\rho = N/L$ is fixed, the density at bulk sites has the form $\langle\tau_1\rangle \simeq \rho\{1-\mathcal{O}(\lambda_B/L)\}$, as we shall see later.

In fact, one can infer most of the results for the ring model with a blockage from section 4, by considering the flux $j = \beta\langle\tau_L\rangle$ across the link $(L, 1)$ as the influx j_0 appearing in (5) for the open system. This relation defines the effective input rate α_e through the relation $j = \alpha_e(1 - \langle\tau_1\rangle)$ and yields in combination with $j = \langle\tau_1\rangle$ in (59),

$$\alpha_e = j/(1 - j) \tag{60}$$

where α_e approaches $\rho/(1-\rho)$ in the thermodynamic limit. The flux across the link $(L, 1)$ can equally be considered as the outflux $\langle\hat{j}_L\rangle = \beta_e\langle\tau_L\rangle$ in (5) of the corresponding open system. This identifies the effective removal rate $\beta_e = \beta$ as the transmission coefficient of the blockage site L.

The phase diagram for the system with a blockage can then be read off from figure 3, showing the flux $j(\rho)$ of the open system at a fixed removal rate β. Consequently, for $\alpha_e < \beta_e$, or equivalently for $j < \beta/(1 + \beta)$ (where $j \sim \rho$ for large systems), the system is in the low-density or free-flow phase. If the density ρ approaches $\rho_F = \beta/(1 + \beta)$, or if α_e approaches β, then the system enters the region of coexisting phases, and the pile-up region, which had before a microscopic width λ_B of approximate size $1/\ln(\beta_e/\alpha_e) = 1/\ln[\beta(1 - \rho)/\rho]$, grows to macroscopic size, as in a wetting transition. For $\rho > \rho_F$ an interface appears downstream of the blockage, at a location R, and the pile-up region has the macroscopic size $L - R$. As the density ρ increases further to $\rho_J = 1/(1 + \beta)$, the location R moves further downstream, according to (see (21))

$$\rho = \left(\frac{R}{L}\right)\frac{\beta}{1+\beta} + \left(1 - \frac{R}{L}\right)\frac{1}{1+\beta} \qquad (\rho_F < \rho < \rho_J). \tag{61}$$

As $\rho \uparrow \rho_J$, the free-flow phase disappears ($R \to 0$), and the system goes into a pure jammed phase, where there is again a microscopic boundary layer, just upstream of the blockage with a deficit density.

In summary, the TASEP on a ring with a blockage site has the following phases,
—free-flow phase: $\rho < \rho_F = \beta/(1+\beta)$
—coexisting phases: $\rho_F < \rho < \rho_J$
—jammed phase: $\rho > \rho_J = 1/(1+\beta)$.

The above results were first obtained and verified against computer simulations by Yukawa *et al* [21].

The density profile $\langle \tau_i \rangle$ in the free-flow phase can be inferred from the corresponding profile (29) for $\alpha_e < \beta_e$, and yields,

$$\begin{aligned} &\langle \tau_i \rangle = j \left\{ 1 + \frac{1-\beta}{\beta} \zeta^{L-i} \right\} \qquad (i < L) \\ &< \tau_L >= j/\beta \end{aligned} \tag{62}$$

where terms of $\mathcal{O}(\zeta^L)$ have been neglected. The relation above is valid for

$$\zeta \equiv \frac{\alpha_e}{\beta_e} = \frac{j}{\beta(1-j)} < 1 \qquad \text{or} \qquad j < \rho_F. \tag{63}$$

In fact, the first line in (62) also covers the case $i = L$. The relation between flux $j(\rho) = \langle \tau_1 \rangle$ and density ρ in the free-flow phase follows by summing (62),

$$\rho = \frac{1}{L} \sum_{i=1}^{L} \langle \tau_i \rangle = j \left\{ 1 + \frac{1}{L} \frac{(1-\beta)(1-j)}{[\beta - j(1+\beta)]} \right\} \tag{64}$$

where $\mathcal{O}(\zeta^L)$-terms have been neglected. The flux $j(\rho)$ can be solved from this quadratic equation, where the root with the minus sign is the physical root. For large systems j differs only slightly from ρ. However, the $\mathcal{O}(1/L)$-correction becomes more and more important as $j \uparrow \rho_F = \beta/(1+\beta)$ where the denominator in (64) diverges. By a perturbation expansion to $\mathcal{O}(1/L)$ we find,

$$j(\rho) = \begin{cases} \rho \left[1 - \left(\dfrac{1-\rho}{\rho_F - \rho} \right) \epsilon \right] & (\rho < \rho_F) \\ \rho_F \left[1 - \left(\dfrac{1}{\rho - \rho_F} \right) \epsilon \right] & (\rho_F < \rho < \frac{1}{2}) \end{cases} \tag{65}$$

with

$$\epsilon = \left(\frac{1-\beta}{1+\beta} \right) \frac{1}{L} \equiv \frac{\Delta\rho}{L} \tag{66}$$

where $\Delta\rho = \rho_J - \rho_F$ is the difference in density between the two coexisting phases. The numerical solution of (64) is plotted in figure 8 as the solid line.

We have again performed computer simulations on large and small systems to test the density dependence of the flux $j(\rho)$. After preparing the system in a random initial configuration, we let the system relax for 4×10^4 timestep, after which it is assumed to be in the NESS. We have calculated time averages over 3×10^5 timesteps, and ensemble averages over 50 different initializations. The agreement in the interval $\rho < \rho_F$ between theory and simulations is excellent, even for small L and β, and for ρ close to ρ_F where the difference between j and ρ is largest, as shown in table 1 and figure 8. For $\rho_F < \rho < \frac{1}{2}$ the difference between theory and simulations becomes somewhat larger. The reason is that equations (62)–(64) are only valid for $\zeta < 1$ or $j < \rho_F$. As soon as $\zeta \simeq 1$ or $j \simeq \rho_F$ equation (64) starts to lose its validity because in (62) and (64) terms of $\mathcal{O}(\zeta^L) \simeq \mathcal{O}(1)$ have been neglected. Simulation results for $j(\rho)$, similar to those in figure 8, have been presented in [21] without a theoretical explanation.

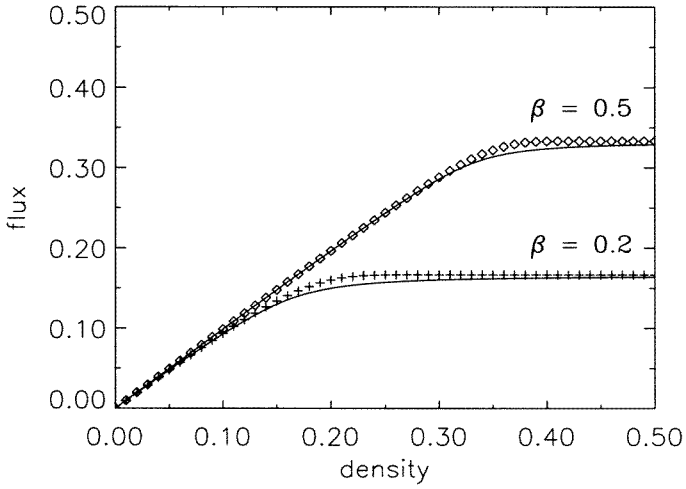

Figure 8. 'Equation of state' for the flux $j(\rho)$ from (64) and (65) (full curve) compared with simulation results for $L = 1000$ sites at $\beta = 0.2$ ($\rho_F \simeq 0.17$) and $\beta = 0.5$ ($\rho_F \simeq 0.33$). The smooth crossover at $\rho = \rho_F$ is derived from the profile (62) of the blockage region.

Table 1. Equation of state $j(\rho, \beta)$.

N	ρ	j(sim)	j(theor)
	$L = 100$	$\beta = 0.25$	$\rho_F = \frac{1}{5}$
10	0.10	0.0955	0.0958
15	0,15	0.1401	0.1384
18	0.18	0.1638	0.1599
	$L = 100$	$\beta = 0.5$	$\rho_F = \frac{1}{3}$
20	0.2	0.1964	0.1962
30	0.3	0.2882	0.2857
	$L = 1000$	$\beta = 0.5$	$\rho_F = \frac{1}{3}$
300	0.30	0.2981	0.2980
330	0.33	0.3243	0.3230
	$L = 100$	$\beta = 0.75$	$\rho_F = \frac{3}{7}$
30	0.30	0.2971	0.2977
40	0.40	0.3914	0.3910
	$L = 1000$	$\beta = 0.1$	$\rho_F = \frac{1}{11}$
60	0.60	0.0587	0.0586
85	0.85	0.0806	0.0797

Next we consider the n-point correlations, which are given through (28) and (16), i.e.

$$\langle \tau_k \tau_{k+1} \dots \tau_{k+n} \rangle = (j/\beta)(1-\beta)^n \zeta^{L-k} \tag{67}$$

with ζ given in (63). This relation also gives the profile $\langle \tau_k \rangle = j + \langle \tau_k \tau_{k+1} \rangle$ of the pile-up region downstream of the blockage. In figure 9 the n-point correlations with $n = 1, 2$ have been compared with computer simulations and again there is good agreement.

Moreover, through arguments similar to those in section 5.1, we conclude that the

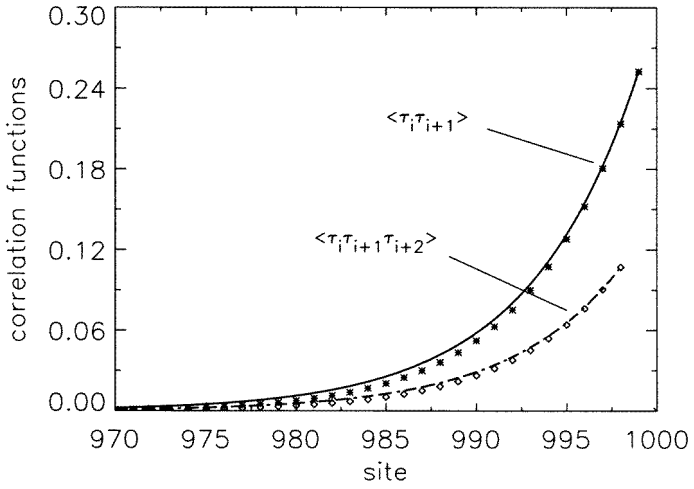

Figure 9. Correlation functions $\langle\tau_i\tau_{i+1}\rangle$ and $\langle\tau_i\tau_{i+1}\tau_{i+2}\rangle$ as a function of i. The points are simulation results; the curve represents the relation (67), with parameters $L = 1000$, $\beta = 0.5$ and $\rho = 0.3$.

probability $P(k)$ to find the first site of the pile up region at site k is proportional to the excess density $\langle\tau_k\tau_{k+1}\rangle$, so that $P(k) = \zeta^{L-k}/(1-\zeta)$. The average width λ_B of the blockage region and the fluctuation $\delta\lambda_B$ around this average are then found from (32) and (33) with ζ given through (63), i.e.

$$\begin{aligned}\lambda_B &= \langle(L-k)\rangle = j/[\beta - j(1+\beta)] \\ (\delta\lambda_B)^2 &= \langle(L-k)^2\rangle - \langle L-k\rangle^2 = \beta j(1-j)/[\beta - j(1+\beta)]^2\end{aligned} \tag{68}$$

where $\langle\cdots\rangle = \sum_k(\ldots)P(k)$. Simulation results for λ_B and $\delta\lambda_B$ have been presented in [21].

For the *high-density* phase all corresponding results can be obtained from particle–hole symmetry. For instance, the profile of the depletion region just upstream of the blockage site L is given by (29) with $\alpha_e = \beta$ and $\beta_e = j/(1-j)$ where $j(\rho,\beta)$ in the jammed phase equals $j(1-\rho,\beta)$ in (64) in the free-flow phase.

The behaviour of the interface in the *coexistence* region is very different from that in the TASEP with *open* boundaries. In the latter the average number of particles $\langle N\rangle$ fluctuates wildly, and the location R of the interface for a given $\alpha = \beta$, can be anywhere on the lattice with equal probability, as the actual density fluctuates between $\beta/(1+\beta)$ and $1/(1+\beta)$. In the TASEP on the ring with blockage the density $\rho = N/L$ is fixed, and R is on average given through (61), and there are only small fluctuations δR around the average R. We have no estimate for the average position and width of the interface between coexisting phases. However, away from coexistence, the profiles of boundary layers in both systems are rather similar. The previous discussion confirms our intuitive interpretation that the TASEP on a ring with a blockage behaves essentially the same as the TASEP with open boundaries with injection rate $\alpha_e = j/(1-j)$ and removal rate $\beta_e = \beta$. This similarity holds for bulk properties, profiles and correlation functions.

7. Conclusion

In this paper, which is in part an account of [22], we have studied the NESS of the TASEP with fully synchronous and *deterministic* ($p = 1$) bulk dynamics (i) for open systems, coupled to particle reservoirs with injection rate α and removal rate β, and (ii) for closed systems on a ring containing a stochastic blockage site with transmission rate β. Mean-field theories and the Boltzmann equation give a totally inadequate description of these far-from-equilibrium states, because of the existence of strong short-range correlations.

As discussed in the introduction, there are many physical processes that can be modelled as TASEPs, such as traffic models. It has been shown in [7] that simple extensions of the present TASEP to stochastic bulk dynamics, to multispeeds, to multilanes, etc—which do not seem to change the basic physics of the model—are able to model realistic traffic flows. Consequently, if traffic systems are operated under NESS conditions with input and output rates close to the jamming transition (here $\alpha = \beta$), then the wild fluctuations in the positions of the tails of large traffic jams (position of the interface or shock wave in Burgers' equation) are intrinsic and physically unavoidable.

It is also of interest to present a more technical comparison of our new method and results with existing ones. The theory presented here is based on two new ideas: (i) starting from the microdynamic equations for the TASEP, we derive the explicit microscopic specifications of the configurations and order parameters for the separate phases; and (ii) we introduce an improved MFA in (25) that neglects fourth- and higher-order correlation functions at the interface between the bulk phase and the boundary layers. The results for the profiles have been compared with extensive computer simulations, and turn out to be indistinguishable from the analytic results. We therefore *conjecture* that our results for the open TASEP with $\alpha \neq \beta$ are *exact* up to terms that are exponentially small in the system size L, for instance of order $(\alpha/\beta)^L$ for $\alpha < \beta$. Our results for the TASEP on the ring with a blockage show small differences between theory and simulations. Clearly the identification of the flux through a blockage as both the influx (to define α_e) *and* the outflux (to define β_e) of the open system is only approximate. Moreover, the neglected correction terms $(\alpha/\beta)^L$ start to become of $\mathcal{O}(1)$ as $\alpha_e \uparrow \beta_e$ or $j \uparrow \rho_F$ (see figure 8).

The first idea has enabled us to obtain exact results not only for bulk densities and currents, but also new results for the spatial and temporal correlation functions. The second idea has enabled us to obtain analytic results for the profiles in the boundary layers of density $\langle \tau_k \rangle$ and cluster correlation functions $\langle \tau_k \tau_{k+1} \ldots \rangle$. For the more general stochastic model with $p < 1$ of [8] no analytic results for profiles and correlation functions are known. The ideas in (i) are akin to the elimination of the 'Garden of Eden' states in [8], and those in (ii) to the 'paradisical MFA', hinted at in [8], but that lingo is not ours.

It is of interest to compare our results for fluxes and bulk densities with known results. The phase diagram has been obtained before in [11, 13] for the same TASEP with sublattice–parallel updating, and in [21] for the fully synchronous TASEP on a ring with a blockage. It has a free-flow phase ($\alpha < \beta$), and a congested phase ($\alpha > \beta$), which coexist when $\alpha = \beta$.

In [8] a more general *stochastic* TASEP with fully synchronous dynamics has been analysed, where particles hop only with probability p (with $p < 1$). The corresponding phase diagram contains the present ($p = 1$) phase diagram for α and β less than $\alpha_c \equiv 1 - \sqrt{1-p}$), but it also contains more phases, such as the maximal current phase. In our ($p = 1$)-model the maximal current phase occurs only as a *bulk* phase for the special parameter values $\alpha = \beta = 1$. In addition, the interface of finite width, separating the coexisting phases for $\alpha = \beta < 1$, constitutes a 'microphase' of maximal current

configurations. In the TASEP with $p = 1$ the interface region (see section 4.2) contains only local configurations common to both the low- *and* high-density phase. These *common* local configurations are identical to the local configurations that constitute the maximal current phase. It would be interesting to find out for the fully synchronous TASEP with $p < 1$ if it is possible to identify an interface region for $\alpha = \beta < \alpha_c$, which constitutes a 'microphase of maximal current configurations' as well.

In the low-density regime ($\alpha < \beta < 1 - \sqrt{1-p}$) of [8] the flux and bulk density are found as

$$j = \alpha \frac{p - \alpha}{p - \alpha^2} \qquad \text{and} \qquad \rho = \frac{\alpha(1-\alpha)}{p - \alpha^2} \tag{69}$$

which reduce for $p = 1$ to the results in (16). The corresponding properties of the phase diagram in the high-density regime can be obtained from particle–hole symmetry.

In order to illustrate the particle–hole attraction in these models, and its dependence on the hopping rate p, we compare our results for the deterministic version ($p = 1$) for the nearest-neighbour correlation functions in the bulk (for $i \ll L - \lambda_R$), i.e.

$$\begin{aligned} &\langle \tau_i \tau_{i+1} \rangle = 0 \qquad \langle \sigma_i \sigma_{i+1} \rangle = 1 - 2\rho \qquad (i \in \text{bulk}) \\ &\langle \tau_i \sigma_{i+1} \rangle = \langle \sigma_i \tau_{i+1} \rangle = j = \rho \qquad (\forall i) \end{aligned} \tag{70}$$

with those for the stochastic version ($p < 1$) in [8], reading

$$\begin{aligned} &\langle \tau_i \tau_{i+1} \rangle = \rho - j/p \qquad (i \in \text{bulk}) \\ &\langle \sigma_i \sigma_{i+1} \rangle = 1 - \rho - j/p \qquad (i \in \text{bulk}) \\ &\langle \tau_i \sigma_{i+1} \rangle = \langle \sigma_i \tau_{i+1} \rangle = j/p \qquad (\forall i) \end{aligned} \tag{71}$$

where relation (6) has been used. Of course (71) includes (70) for $p = 1$.

Note that in the low-density phase of the deterministic version there is a 'hard core repulsion' for nearest-neighbour sites, as $\langle \tau_i \tau_{i+1} \rangle = 0$ or equivalently, a strong attraction of particle–hole pairs on nearest-neighbour sites. In the stochastic version ($p < 1$) there is also a particle–hole attraction on nearest-neighbour sites, because the covariance

$$\langle \tau_i \sigma_{i+1} \rangle - \langle \tau_i \rangle \langle \sigma_{i+1} \rangle = \frac{\alpha^2 (p - \alpha)^2}{p(p - \alpha^2)} > 0 \tag{72}$$

i.e. there exists a positive correlation between an occupied site and the empty site, just in front of it, which increases monotonically as $p \uparrow 1$.

It would be very valuable to extend this method, based on the ideas summarized in (i) and (ii) at the start of this section, to calculate the profiles, and spatial and temporal correlation functions in the stochastic TASEP of [8] with its much richer phase diagram containing a maximal current phase.

Acknowledgments

MHE would like to thank H Knops for stimulating discussions and A Schadschneider for clarifying correspondence.

Appendix. Sublattice–parallel dynamics

We will now illustrate how the method of this paper, when applied to the TASEP with sublattice–parallel updating, yields the exact results for the bulk properties and the asymptotic (large system) results for profiles and correlation functions, as obtained in

[11, 13] The dynamics consists of two substeps. In the first step from $t \to t' = t + \frac{1}{2}$, the pairs $(1, L), (23), \ldots, (L-2, L-1)$ are updated in parallel where L is even. There is only a possibly nonvanishing microscopic flux $\hat{j}_i$ through the *even* link $(i, i+1)$, whereas the flux $\hat{j}_i$ through the *odd* link vanishes. In the second step, from $t \to t'' = t' + \frac{1}{2} = t + 1$, the pairs (1,2), (3,4), $\ldots, (L-1, L)$ are updated in parallel, then $\hat{j}_{i+1}$ is possibly nonvanishing and $\hat{j}_i$ vanishes.

If we denote $\tau_a(t), \tau_a(t + \frac{1}{2})$ and $\tau_a(t+1)$ respectively by τ_a, τ'_a and τ''_a with $a = \{1, 2, \ldots, L\}$, then the *microdynamic* equation for the first step $t \to t'$ becomes:

$$\begin{aligned} \tau'_i &= \tau_i \tau_{i+1} \qquad (0 < i \leqslant L; i \text{ even}) \\ \tau'_{i+1} &= \tau_{i+1} + \tau_i \sigma_{i+1} \qquad (0 \leqslant i < L; i \text{ even}) \end{aligned} \tag{A1}$$

and for the second step $t' \to t + 1$

$$\begin{aligned} \tau''_i &= \tau'_i + \tau'_{i-1}\sigma'_i \qquad (0 < i \leqslant L; i \text{ even}) \\ \tau''_{i+1} &= \tau'_{i+1}\tau'_{i+2} \qquad (0 \leqslant i < L; i \text{ even}). \end{aligned} \tag{A2}$$

With the conventions $\tau_0 = \hat{\alpha}$ and $\sigma_{L+1} = \hat{\beta}$, as defined below (2), these equations also include the boundary conditions for the open system. Moreover, we observe that the evolution equations (A1), (A2) are invariant under the particle–hole exchange.

In the NESS there is again a constant site-independent flux through the system. The flux $\langle \hat{j}_i \rangle$ out of *even* sites at integer times is equal to the flux $\langle \hat{j}'_{i+1} \rangle$ out of *odd* sites at half-integer times, i.e.

$$\begin{aligned} j &= \langle \hat{j}_i \rangle = \langle \tau_i \sigma_{i+1} \rangle \\ &= \langle \hat{j}'_{j+1} \rangle = \langle (\tau_{i+1} + \tau_i \sigma_{i+1})(\sigma_{i+2} + \tau_{i+2}\sigma_{i+3}) \rangle \end{aligned} \tag{A3}$$

where $\tau_0 = \widehat{\alpha}$ and $\sigma_L = \widehat{\beta}$ and i is *even*.

By studying the dynamics of clusters as in section 3 one finds that (A1) and (A2) impose some very strong constraints on the allowed configurations, i.e.

$$\begin{aligned} &(\tau\sigma)''_{i-1,i} = \tau'_{i-1}\tau'_i\sigma'_{i-1}\sigma'_i = 0 \\ &(\tau\tau\sigma\sigma)''_{i-1,i+2} = \tau'_{i-1}\tau'_i\sigma'_{i+1}\sigma'_{i+2} = \{(\tau\tau\tau)_{i-1,i+1} + (\tau\sigma\tau\tau)_{i-2,i+1}\}\sigma_i\sigma_{i+1}\tau_{i+2}\tau_{i+3} = 0. \end{aligned} \tag{A4}$$

This implies that configurations containing $(\ldots 10_+ \ldots)$ and $(\ldots 1100_+ \ldots)$ can never be created at integer times if one starts from an empty initial state. Such configurations are therefore *absent* in the NESS for *any* value of α and β. The subscripts $(\pm)$ on $\tau_\pm$ indicate that the relevant site has an *even* (+) or an *odd* $(-)$ label. Of course configurations $(\ldots 10_- \ldots)$ as well as $(\ldots 0011 \ldots)$ are allowed at integer times.

Moreover, by arguments similar to those in sections 3.1 and 3.2, one shows again that the first particle cluster can only be created at the exit site. Let k_0 be the location of the last particle on the last cluster of particles, then the interval downstream of k_0 contains only *isolated particles*, separated by holes (free-flow configurations with interval density $\rho(< k_0) < \frac{1}{2}$), and that upstream of k_0 contains only *isolated holes* (jammed configurations with interval density $\rho(> k_0) > \frac{1}{2}$). All conclusions in the last three paragraphs of section 3.1 carry over to the TASEP with sublattice–parallel dynamics, as does the phase diagram.

Next, we consider the bulk properties for large systems ($L \to \infty$) in the free-flow phase ($\alpha < \beta$ and $\rho_F < \frac{1}{2}$). The low-density phase is again characterized by the microscopic order parameter $\tau_i \tau_{i+1} = 0$. To perform these calculations, we start, as in section 4.1, from the constant flux relations (A3) in combination with the vanishing order parameter,

$$j = \langle \hat{j}_i \rangle = \langle \tau_2 \rangle = \cdots = \langle \tau_i \rangle = \beta \langle \tau_L \rangle$$

$$= \langle \hat{j}'_{i+1} \rangle = \alpha(1 - \langle \tau_1 \rangle) = \langle \tau_2 + \tau_3 \rangle$$
$$= \cdots = \langle \tau_i + \tau_{i+1} \rangle \tag{A5}$$

valid for $i \ll L - \lambda_R$ and i even. This implies for *odd bulk* sites $\langle \tau_- \rangle = 0$, and for *even bulk* sites $\langle \tau_+ \rangle = \alpha$ and $\langle \tau_L \rangle = \alpha/\beta$. If $\langle j_+ \rangle$ denotes the flux out of even bulk sites, and $\langle j_- \rangle$ the one out of odd sites, then the results for the free-flow phase ($\alpha < \beta$) can be summarized as,

$$\begin{aligned} &\langle \tau_+ \rangle = \alpha \qquad \langle \tau_- \rangle = 0 \qquad \langle \tau_L \rangle = \alpha/\beta \\ &\langle \hat{j}_+ \rangle = \alpha \qquad \langle j_- \rangle = 0. \end{aligned} \tag{A6}$$

The corresponding relations for the jammed phase ($\alpha > \beta$) can be obtained from the relations (8) for particle–hole symmetry, and read

$$\begin{aligned} &\langle \tau_+ \rangle(\alpha, \beta) = 1 - \langle \tau_- \rangle(\beta, \alpha) = 1 \\ &\langle \tau_- \rangle(\alpha, \beta) = 1 - \langle \tau_+ \rangle(\beta, \alpha) = 1 - \beta \\ &\langle \tau_1 \rangle(\alpha, \beta) = 1 - \langle \tau_L \rangle(\beta, \alpha) = 1 - \beta/\alpha \end{aligned} \tag{A7}$$

and for the fluxes, using (9),

$$\begin{aligned} &\langle \hat{j}_+ \rangle(\alpha, \beta) = \langle \hat{j}_+ \rangle(\beta, \alpha) = \beta \\ &\langle \hat{j}_- \rangle(\alpha, \beta) = 0. \end{aligned} \tag{A8}$$

Next, we consider the profile in the right boundary layer of the *low-density* phase, and we construct the dynamics of the cluster functions T, as in (11). By specializing these equations to the low-density phase one arrives after lengthy, but straightforward algebra, at a coupled hierarchy of equations for the correlation functions.

Let i or $i + 1$ (with i = even) be the last particle position on the last particle cluster, then we find in the NESS the exact relations,

$$\begin{aligned} \langle T_{ik} \rangle &= \langle T_{i,k-1} \rangle = \langle T_{i,k+1} \rangle + \langle (\tau\sigma\sigma T)_{i-2,k+1} \rangle + \langle (\tau\sigma\tau\sigma T)_{i-2,k+1} \rangle \\ \langle T_{i+1,k} \rangle &= \langle T_{i+1,k-1} \rangle = \langle T_{i+1,k+1} \rangle + \langle (\tau\sigma T)_{i,k+1} \rangle \end{aligned} \tag{A9}$$

where i and k are both *even*. The present set of coupled equations is the analogue of (24). By application of the mean-field assumption, formulated in (24) and (25), the above set of equations simplifies to the set of recursion relations with i and k even,

$$\begin{aligned} \langle T_{ik} \rangle &= \langle T_{i,k+1} \rangle + \alpha \langle T_{i+1,k+1} \rangle + \alpha^2 \langle T_{i+2,k+1} \rangle \\ \langle T_{i+1,k} \rangle &= \langle T_{i+1,k+1} \rangle + \alpha \langle T_{i+2,k+1} \rangle. \end{aligned} \tag{A10}$$

The boundary condition for this set is included by setting $k = L$.

Our special mean-field assumption for the *low-density* phase neglects again higher-order correlations between on the one hand the particle–hole pairs $\tau\sigma$ and $\tau\sigma\tau\sigma$, and on the other hand the tailing particle cluster at the interface of bulk phase and boundary layer. The solution of these recursion relations yields

$$\begin{aligned} \langle T_{ik} \rangle = \langle T_{i,k-1} \rangle &= \frac{\alpha}{\beta} \langle T_{i+1,k} \rangle = \frac{\alpha}{\beta} \langle T_{i+1,k+1} \rangle \\ &= \left(\frac{\alpha}{\beta} \right)^{L-i+1} (1 - \beta)^{\frac{1}{2}(k-i)}. \end{aligned} \tag{A11}$$

From these results and from (6) we obtain the density profile of the boundary layer near the exit for *even* sites i,

$$\langle \tau_i \rangle = \alpha + (1 - \beta) \left(\frac{\alpha}{\beta} \right)^{L-i+1}. \tag{A12}$$

For *odd* sites $i+1$ follows similarly,

$$\langle \tau_{i+1} \rangle = (1-\beta)\left(\frac{\alpha}{\beta}\right)^{L-i}. \tag{A13}$$

The results for the profiles and correlation functions (A11)–(A13) are in full agreement with the *exact* results of [11, 13] for large systems, when terms of order $(\alpha/\beta)^L$ have been neglected.

In close parallel to section 5.2, we may also calculate the spatial and temporal correlation functions in the bulk of the low-density phase. By setting the microscopic order parameter $\tau_i \tau_{i+1} = 0$ in (A1), (A2), the microdynamic equation for bulk sites ($i \ll L - \lambda_R$) reduces to

$$\tau_i(t+1) = \tau_{i-2}(t) \qquad \tau_{i+1}(t) = 0 \tag{A14}$$

where i is even. The correlation function in the NESS with i and R even are then,

$$\begin{aligned} \langle \tau_{i+R}(t)\tau_i(0)\rangle &= \langle \tau_{i+R-2t}(0)\tau_i(0)\rangle \\ &= \langle \tau_{i+R}(t)\rangle\langle \tau_i\rangle = \alpha^2 \end{aligned} \tag{A15}$$

holding for $0 \leqslant \{i, j\} \ll L - \lambda_R$ with $j = i + R - t$ and $R \neq 2t$. For i and/or R odd, the correlation function vanish, as $\langle \tau \rangle = 0$ for *odd* sites. We observe that the occupations between two even sites in the low-density phase are *uncorrelated*, as a consequence of the *sublattice–parallel* dynamics. In the corresponding case of fully parallel dynamics, the occupations are *correlated*, as is shown in (44) and (46). The absence of correlation is understandable here, as a particle, attempting to enter the system in the low-density phase at site 1 is never blocked.

References

[1] Dorfman J R and Kirkpatrick T R 1980 *Systems Far From Equilibrium (Lecture Notes in Physics 132)* ed L Garrido (Berlin: Springer) p 263
Dorfman J R, Kirkpatrick T R and Sengers J V 1994 *Ann. Rev. Phys. Chem.* **45** 213
[2] Schmittmann B and Zia R K P 1995 *Statistical Mechanics of Driven Diffusive Systems* (London: Academic)
[3] Spohn H 1991 *Large Scale Dynamics of Interacting Particles* (Berlin: Springer)
[4] Grinstein G, Lee D-H and Sachdev S 1990 *Phys. Rev. Lett.* **64** 1927
Grinstein G 1991 *J. Appl. Phys.* **69** 5441
[5] van Noije T P C, Ernst M H, Brito R and Orza J A G 1997 *Phys. Rev. Lett.* **79** 411
[6] Ernst M H and Bussemaker H J 1995 *J. Stat. Phys.* **81** 515
Bussemaker H J and Ernst M H 1996 *Phys. Rev.* E **53** 5837
[7] Schreckenberg M, Schadschneider A, Nagel K and Ito N 1995 *Phys. Rev.* E **51** 2339
[8] Rajewsky N, Santen L, Schadschneider A and Schreckenberg M 1997 *Preprint* cond-mat/9710316
Rajewski N 1997 Exact results for one-dimensional stochastic processes *PhD Dissertation* (Köln University)
[9] Derrida B, Domany E and Mukamel D 1992 *J. Stat. Phys.* **69** 667
Derrida B and Evans M R 1997 *Nonequilibrium Statistical Mechanics in One-dimension* ed V Privman (Cambridge: Cambridge University Press) ch 4
[10] Schütz G and Domany E 1993 *J. Stat. Phys.* **72** 277
[11] Schütz G M 1993 *Phys. Rev.* E **47** 4265
[12] Honecker A and Peschel I 1997 *J. Stat. Phys.* **88** 319
[13] Hinrichsen H 1996 *J. Phys. A: Math. Gen.* **29** 3659
[14] Janowsky S A and Lebowitz J L 1992 *Phys. Rev.* A **45** 618
Janowsky S A and Lebowitz J L 1994 *J. Stat. Phys.* **77** 35
[15] Schütz G 1993 *J. Stat. Phys.* **71** 471
[16] Mallick K 1996 *J. Phys. A: Math. Gen.* **29** 5375
[17] Evans M R 1997 *J. Phys. A: Math. Gen.* **30** 5669
[18] Hinrichsen H and Sandow S 1997 *J. Phys. A: Math. Gen.* **30** 2745

[19] Schadschneider A and Schreckenberg M 1993 *J. Phys. A: Math. Gen.* **26** L679
[20] Stinchcombe R B and Schütz G M 1995 *Phys. Rev. Lett.* **75** 140
[21] Yukawa S, Kikuchi M and Tadaka S 1994 *J. Phys. Soc. Japan* **63** 3609
[22] Tilstra L G and Ernst M H 1997 Driven nonequilibrium systems: traffic flow models *Master Thesis* Utrecht Universiteit
[23] Frisch U, d' Humieres D, Hasslacher B, Lallemand P, Pomeau Y and Rivet J P 1989 *Lattice Gas Methods for Partial Differential Equations* ed G D Doolen (Reading, MA: Addison-Wesley) p 75